MULTISCALE MODEL. SIMUL.
Vol. 18, No. 2, pp. 1076–1112

PHASE FIELD MODELING OF PRECIPITATION AND DISSOLUTION PROCESSES IN POROUS MEDIA: UPSCALING AND NUMERICAL EXPERIMENTS*

CARINA BRINGEDAL†, LARS VON WOLFF‡, AND IULIU SORIN POP§

Abstract. We consider a model for precipitation and dissolution in a porous medium, where ions transported by a fluid through the pores can precipitate at the pore walls and form mineral. Also, the mineral can dissolve and become part of the fluid as ions. These processes lead to changes in the flow domain, which are not known a priori but depend on the concentration of the ions dissolved in the fluid. Such a system can be formulated through conservation equations for mass, momentum, and solute in a domain that evolves in time. In this case the fluid and mineral phases are separated by a sharp interface, which also evolves. We consider an alternative approach by introducing a phase field variable, which has a smooth, diffuse transition of nonzero width between the fluid and mineral phases. The evolution of the phase field variable is determined through the Allen–Cahn equation. We show that as the width of the diffuse transition zone approaches zero, the sharp-interface formulation is recovered. When we consider a periodically perforated domain mimicking a porous medium, the phase field formulation is upscaled to Darcy scale by homogenization. Then, the average of the phase field variable represents the porosity. Through cell problems, the effective diffusion and permeability matrices are dependent on the phase field variable. We consider numerical examples to show the behavior of the phase field formulation. We show the effect of flow on the mineral dissolution, and we address the effect of the width of the diffuse interface in the cell problems for both a perforated porous medium and a thin strip.

Key words. porous media, phase field model, reactive transport, homogenization

AMS subject classifications. 35C20, 35L65, 65M08, 76D05, 76M50, 76R50, 76S05, 76V05, 80A22, 80A32

DOI. 10.1137/19M1239003

1. Introduction.

Understanding mineral dissolution and precipitation processes in porous media is important, as these processes appear in many applications of highest societal relevance. Examples in this sense are soil salinization, geological CO_2 sequestration, copper leaching, and harnessing geothermal energy. In many of these situations, experiments are unfeasible or even impossible, and hence creating simulations based on reliable and accurate mathematical modeling is a key strategy. The most challenging aspect of mathematical modeling appears when the flow domain is

*Received by the editors January 15, 2019; accepted for publication (in revised form) March 5, 2020; published electronically June 11, 2020.
https://doi.org/10.1137/19M1239003
Funding: The authors were supported by the Research Foundation – Flanders (FWO) through the project G0G1316N DynScale through the Odysseus programme, and by the Deutsche Forschungsgemeinschaft (DFG, German Research Foundation) through project 327154368 – SFB 1313. The second author was supported by Hasselt University through the project BOF19BL12. The computational resources and services used in this work were provided by the VSC (Flemish Supercomputer Center), funded by the Research Foundation – Flanders (FWO) and the Flemish Government – department EWI.

†Faculty of Sciences, Hasselt University, Diepenbeek, BE3590, Belgium, and Institute for Modelling Hydraulic and Environmental Systems, University of Stuttgart, 70569 Stuttgart, Germany (carina.bringedal@iws.uni-stuttgart.de).
‡Institute of Applied Analysis and Numerical Simulation, University of Stuttgart, 70569 Stuttgart, Germany, and Faculty of Sciences, Hasselt University, Diepenbeek, BE3590, Belgium (lars.von-wolff@mathematik.uni-stuttgart.de).
§Faculty of Sciences, Hasselt University, Diepenbeek, BE3590, Belgium, and Department of Mathematics, University of Bergen, N-5020 Bergen, Norway (sorin.pop@uhasselt.be).

altered due to dissolution and precipitation. More precisely, the dissolved ions can form a mineral, and hence they can leave the fluid domain and become part of the stationary mineral domain. Due to this, the space available for flow (the fluid domain) is reduced, whereas the mineral domain is increasing. In contrast, the mineral domain shrinks as minerals dissolve into ions and become part of the fluid. To mathematically model such processes one needs conservation laws for mass, momentum, and solute in two time-dependent domains, where the evolution of the interface separating these domains is not known a priori. Hence, we have a free boundary problem, where the development of the boundary—and hence also the domains—must be accounted for.

When encountered in a porous medium, mineral precipitation and dissolution can significantly alter the pore structure and hence affect the porosity and the large-scale flow through the medium as the permeability evolves. For porous media flow, we distinguish between two spatial scales. The detailed behavior is found at the pore scale (the microscale), and the average behavior of the system is considered to be at the Darcy scale (the macroscale). Mineral precipitation and dissolution at the Darcy scale have been considered from a theoretical point of view by [25], where consistent reaction rates are formulated for the dissolution and precipitation processes, and traveling wave solutions are found. The existence and uniqueness of such solutions are further analyzed in [44]. At the pore scale, the existence of weak solutions is proved in [46], while uniqueness is obtained in [51]. Paper [46] also analyzes the occurrence of dissolution fronts in a thin strip, introducing a free boundary separating regions where mineral is present from those which are mineral-free. In [26], homogenization techniques are employed to prove rigorously that the Darcy-scale model in [25, 44] is the upscaled counterpart of the pore-scale model in [46].

In all of the cases mentioned above, the mineral layer is assumed to have a negligible thickness even when compared to the microscale (the pores), and therefore the presence of a mineral is accounted for in the form of a concentration. A different approach is adopted in [50], where the mineral layer is assumed to have a nonnegligible thickness, and therefore precipitation and dissolution can alter the flow domain at the microscale. The existence and uniqueness of a weak solution for this free boundary model is proved, however, in the simplified case of a one-dimensional domain. This situation has extended to the higher dimensional case. In [48] the pore-scale model is defined in a two-dimensional thin strip, where a free boundary model for precipitation and dissolution is included. The Darcy-scale model is derived by transversal averaging. Paper [47] extends this by considering a general porous medium with periodic grains, and a level-set formulation is used to account for the presence of the free boundary at the pore scale. These models were later extended to include temperature dependence for a thin strip [10] and for a periodic porous medium [11], and the effective properties of the latter model were considered further in [13]. Also, the upscaling in advection-dominated regimes, leading to models that are similar to Taylor dispersion, is performed in [12, 28]. A similar model is considered in [43] but restricted to pore-scale diffusion processes in evolving domains. There a Darcy-scale model is derived, for which the existence of strong solutions is proved up to clogging.

Different approaches are possible when considering free boundary models. One can formulate an explicit equation for the location of the free boundary through, e.g., the width of the mineral phase in a thin strip as in [12, 10, 28, 48, 50]. For more general geometries, a level-set formulation has been widely used, as in [11, 43, 47]. Upscaling using asymptotic expansions of level-set formulations can be tedious due to the strong coupling between the level-set equation and the other model equations, as the asymptotic expansion has to be applied also for the level set and hence for the

location of the interface, as done in [11, 43, 47]. However, the upscaled model still relies on solving the pore-scale level-set equation, which is quite challenging for the numerical implementation.

To obtain mathematical models valid at the Darcy scale, asymptotic expansion and homogenization techniques (see, e.g., [23]) are employed in the above-mentioned papers. This is the strategy adopted in the current paper as well. Alternatively, one can consider volume averaging techniques [36, 37, 52, 53, 54]. We refer the reader to [19] for a comparison between the two methods. We mention that the results are obtained under the assumption that diffusion is the result of a standard random walk process at the molecular scale. Alternatively, one can start with a continuous time random walk (CTRW) approach [29] and end up with other diffuse regimes, expressed, e.g., through fractional time derivatives. Considering such models, including the upscaling from the pore to the Darcy scale (see [20]) is certainly interesting but is beyond the scope of the current work.

Darcy-scale models are derived through assuming a certain relation between the time scales of the different processes (diffusion, advection, reaction) at the pore scale, where different relations lead to different upscaled models. These time scales are assumed either to be in balance or to differ in a certain way. This can be expressed through the order of magnitude of dimensionless numbers, such as Péclet and Damköhler numbers, in terms of the ratio of the typical length scales of the pores, respectively, of the porous medium (the Darcy scale). In this work we will assume these time scales to be in balance. The resulting Darcy-scale model reflects nonequilibrium chemical kinetics. Certainly, equilibrium kinetics may appear at the scale of pores, in which case one needs to adapt the mathematical models at the pore scale, with impact on the upscaled ones (see, e.g., [7]). Homogenization techniques can still be employed in other regimes, including high Péclet and Damköhler numbers, but, in particular, the former needs to remain within a regime that avoids turbulent flows and allows diffusion to dominate at the scale of pores. We mention [4, 6, 12, 17, 28, 32, 36, 45, 53, 54] for the derivation of Darcy-scale models by either homogenization or volume averaging, and under dominating advection or for fast reaction kinetics. A comprehensive discussion can be found in [7], addressing models with mixing-controlled heterogeneous reactions at different scales and under various regimes for the Péclet and Damköhler numbers.

To model the evolving fluid-mineral interface, an alternative approach to the level-set method is through phase fields. A phase field is an approximation of the characteristic function and hence attains the value 1 in one domain, and 0 in the other, but has a smooth, diffuse transition zone of nonzero width across the interface [14, 30]. The evolution of the phase field is through a phase field equation, which can be derived from a minimization of the free energy. Most commonly used are the Allen–Cahn [5] and Cahn–Hilliard [15] equations for evolution of the phase field. While the Cahn–Hilliard equation has the advantage of conserving the phase field parameter, it introduces fourth-order spatial derivatives which can lead to numerical difficulties. For the Allen–Cahn formulation, one can prove that the phase field remains bounded by 0 and 1 and thus in the physical regime, as it involves only second-order derivatives. On the other hand, it is generally not conservative, although conservative reformulations for two-phase flow [24] and multicomponent systems [35] exist. However, these formulations are globally rather than locally conservative. The Allen–Cahn equation allows the interface to evolve due to curvature effects (the Gibbs–Thomson effect), which may or may not be desirable from a chemical point of view [40]. We will use an Allen–Cahn equation for our phase field formulation, although curvature effects are

not our primary point of interest. We mention that [55] formulated an Allen–Cahn equation for a solid-liquid interface evolving due to solute precipitation and dissolution, where surface curvature effects were removed. However, the model does not include fluid flow.

To introduce a diffuse transition zone, the model equations (i.e., the conservation of mass, momentum, and solute) need to be reformulated in the combined domain of fluid and mineral in a consistent manner. The combined domain is then stationary. This reformulated model has to incorporate the boundary conditions of the original model at the evolving interface as part of the model equations. An essential property of a phase field formulation is that the corresponding sharp-interface formulation (i.e., the original model equations and boundary conditions at the evolving interface) is recovered when the width of the diffuse interface approaches zero [21, 30]. This limit can be investigated using matched asymptotic expansions [14].

Considering mineral precipitation and dissolution, [49] proposed a phase field formulation based on the Allen–Cahn equation for the movement of the solid-liquid interface but without flow in the fluid phase. Later [38] extended an equivalent formulation of [49] to include two fluid phases—with curvature effects between them—but still without flow. There, the interfaces are moving due to curvature effects. An Allen–Cahn formulation for two-phase Stokes flow with curvature effects on the evolving fluid-fluid interface, but without chemical reactions, was formulated in [1]. A Cahn–Hilliard model for two fluid phases and a solid phase, including mineral precipitation, is proposed in [39]. Using matched asymptotic expansion techniques, in each of these four papers it is shown that the phase field models reduce to the corresponding sharp-interface models. The aim in this paper is to formulate a phase field model for mineral precipitation and dissolution, in which the flow of a fluid phase transporting the precipitating solute is also taken into account. The model builds on the ones in [38, 49]. Compared to [1], where the moving interface separates two mobile fluid phases, the current moving interface separates a mobile phase (the fluid) and an immobile (mineral) phase. Therefore, the formulation in [1] cannot be applied here. In this respect, the present situation is more similar to the melt convection model considered in [8], where the interface between stationary solid and flowing fluid is evolving due to melting. However, [8] did not consider the sharp-interface limit for their phase field formulation.

This paper is organized as follows. In section 2 the phase field formulation is introduced, based on the sharp interface formulation. Next, in section 3 we show that the phase field formulation reduces to the sharp-interface formulation when the width of the diffuse interface approaches zero. Two numerical examples showing the behavior of the phase field formulation are included in section 4. In particular, we show how the flow affects the dissolution process. Then homogenization techniques are applied in section 5 to derive a Darcy-scale counterpart for a specific setting of the phase field model. Finally, section 6 provides some further numerical examples: First, we study the behavior of the upscaled model parameters in terms of the diffuse interface parameter, and then the convergence of the homogenization process for a simplified situation, where the model is defined in a thin strip.

2. Formulation of the reactive transport problem. Before introducing the phase field formulation, first we formulate the corresponding sharp-interface model including a free boundary. Both models are restricted to the case where only one fluid phase is present, which, in the case of a porous medium, can be seen as a single-phase, fully saturated flow. Moreover, the density and viscosity of the fluid are

assumed constant. Furthermore, we only consider a simplified electrochemical system, where the precipitate is formed at the boundaries of the flow domain (the pore walls) and is the product of the reaction between two ions diffusing into and transported by the flowing fluid. If the diffusion coefficients of the two ions are the same, and if the system is electroneutral, one can simplify the chemistry by only considering one equation for the solute concentration, as knowing the concentration of one solute and using the electroneutrality of the system enables us to obtain the other concentration straightforwardly (see [25, 46, 50]).

The models below are given in a dimensional framework. The nondimensionalization is discussed later in subsection 5.2.

2.1. Sharp-interface formulation. We start with the sharp-interface formulation, which later motivates the phase field model. In this case, we let Ω denote the entire domain (the porous medium), which is divided into two disjoint subdomains: one occupied by the fluid, and the other occupied by the mineral. The mineral layer is the result of precipitation and dissolution and therefore has a variable thickness that is not known a priori. Hence, the domains occupied by the fluid and the mineral are both time dependent. Letting $t \geq 0$ stand for the time variable and denoting by $\Omega_f(t)$ the (time-dependent) fluid domain, the conservation laws for the fluid and its momentum and for the solute are

$$\nabla \cdot \mathbf{q} = 0 \qquad \text{in } \Omega_f(t), \tag{2.1a}$$

$$\rho_f \partial_t \mathbf{q} + \rho_f \nabla \cdot (\mathbf{q} \otimes \mathbf{q}) + \nabla p = \mu_f \nabla^2 \mathbf{q} \qquad \text{in } \Omega_f(t), \tag{2.1b}$$

$$\partial_t u + \nabla \cdot (\mathbf{q} u) = D \nabla^2 u \qquad \text{in } \Omega_f(t). \tag{2.1c}$$

Here $\mathbf{q}$ is velocity and p is pressure in the fluid, and ρ_f and μ_f are the constant density and viscosity of the fluid. Finally, u is solute concentration and D its diffusivity.

In the mineral domain $\Omega_m(t)$, the mineral is immobile and has a constant concentration u^*, which reduces (2.1a)–(2.1c) to

$$\mathbf{q} = \mathbf{0} \quad \text{ in } \Omega_m(t).$$

In what follows, we assume that the concentration in the mineral is always larger than the one in the fluid, namely $u^* > u(x,t)$ for all $t \geq 0$ and $x \in \Omega_f(t)$.

We let $\Gamma(t)$ stand for the free boundary separating $\Omega_f(t)$ and $\Omega_m(t)$. Observe that for any time t, one has

$$\Omega = \Omega_f(t) \cup \Omega_m(t) \cup \Gamma(t) \quad \text{and} \quad \Omega_f(t) \cap \Omega_m(t) = \emptyset.$$

At $\Gamma(t)$, to guarantee the mass balance we adopt the Rankine–Hugoniot boundary conditions for the fluid and the solute. We assume that the chemistry does not lead to any volume change, which means that one mineral mole takes exactly the same volume as the one occupied in the fluid by the ion moles forming the mineral (see [11, 47]). With this, the conditions at the moving interface are

$$v_n + \gamma \kappa = -\frac{1}{u^*} f(u) \qquad \text{on } \Gamma(t), \tag{2.2a}$$

$$\mathbf{q} = \mathbf{0} \qquad \text{on } \Gamma(t), \tag{2.2b}$$

$$v_n (u^* - u) = \mathbf{n} \cdot D \nabla u \qquad \text{on } \Gamma(t), \tag{2.2c}$$

where v_n is the speed of the moving interface in the normal direction $\mathbf{n}$ pointing into the mineral, γ is the diffusivity of the interface, and κ is the curvature of the moving interface.

Observe that (2.2a) is describing the movement of the free boundary due to precipitation and dissolution. More precisely, the function f is the difference between the precipitation rate and the dissolution rate. Without being restricted to this choice, we use a simple reaction rate inspired by the mass action kinetics, namely,

$$f(u) = f_p(u) - f_d = k\left(\frac{u^2}{u_{\text{eq}}^2} - 1\right), \tag{2.3}$$

where u_{eq} is the (known) equilibrium concentration for which $u^* > u_{\text{eq}}$, and k is a reaction constant of dimension $\frac{\text{mol}}{\text{m}^2\ \text{s}}$. This choice of reaction rate corresponds to a precipitation rate increasing with ion concentration and a constant dissolution rate. Note that to avoid dissolution whenever no mineral is present, in [25, 46] the dissolution rate is given as a multivalued rate involving the Heaviside graph.

As follows from (2.2a), next to the precipitation and dissolution, the free boundary is also moving due to surface curvature. The latter effect is more common for two-phase flow but can also occur for interfaces separating a fluid from a solid phase. This assumption is natural when minimizing the free energy of the surface [2, 40]. In our case, γ will be very small.

The last two conditions at $\Gamma(t)$ ensure the mass balance for the fluid and the solute. Since we assume no volume change in connection with the chemistry, the normal component of the fluid velocity is zero at the moving boundary. Combined with the no-slip condition, it follows that the fluid velocity $\mathbf{q}$ is zero at the moving boundary. Finally, (2.2c) is the Rankine–Hugoniot condition for the ions. The flux on the right-hand side is due to diffusion as the convective flux is zero, following from (2.2b). Also, the mineral is immobile, so the flux in the mineral subdomain is 0, whereas the concentration u^* is fixed.

For completeness we mention that the location of the moving interface $\Gamma(t)$ can be determined as the 0 level set of a function $S : \Omega \times [0, \infty) \to \mathbb{R}$ satisfying

$$S(x,t) = \begin{cases} < 0 & \text{if } x \in \Omega_f(t), \\ 0 & \text{if } x \in \Gamma(t), \\ > 0 & \text{if } x \in \Omega_m(t). \end{cases}$$

Then, S satisfies the equation

$$\partial_t S + v_n |\nabla S| = 0 \quad \text{for } x \in \Omega.$$

The level-set approach is adopted in [11, 13, 43, 47].

2.2. Phase field formulation. An alternative to the sharp-interface formulation given above is to consider a phase field formulation. In this case, one uses a phase field, which is an approximation of the characteristic function. The nondimensional phase field ϕ is close to and approaches 1 in the fluid phase, is close to and approaches 0 in the mineral, and has a smooth transition of (dimensional) width $O(\lambda) > 0$ separating the phases. In other words, $\lambda > 0$ is a phase field parameter related to the thickness of the diffusive transition region. It is to be expected that when passing λ to 0, one obtains in the limit the original sharp-interface model. In consequence, the phase field approach replaces the interface between the two phases by a smooth transition region where diffusive effects are included. The advantage is that the model equations can now be defined on a stationary domain (here Ω) instead of on time-evolving domains. This approach, however, requires the flow and transport equations

to also be defined in the mineral phase. Here we extend the phase field models in [38, 49] as follows to include flow:

$$\lambda^2 \partial_t \phi + \gamma P'(\phi) = \gamma \lambda^2 \nabla^2 \phi - 4\lambda \phi(1-\phi) \frac{1}{u^*} f(u), \tag{2.4a}$$

$$\nabla \cdot (\phi \mathbf{q}) = 0, \tag{2.4b}$$

$$\rho_f \partial_t (\phi \mathbf{q}) + \rho_f \nabla \cdot (\phi \mathbf{q} \otimes \mathbf{q}) = -\phi \nabla p + \mu_f \phi \nabla^2 (\phi \mathbf{q}) - g(\phi, \lambda)\mathbf{q} + \frac{1}{2} \rho_f \mathbf{q} \partial_t \phi, \tag{2.4c}$$

$$\partial_t \big(\phi(u - u^*)\big) + \nabla \cdot (\phi \mathbf{q} u) = D \nabla \cdot (\phi \nabla u). \tag{2.4d}$$

The model is explained in detail below.

2.2.1. Comments on the phase field equation (2.4a). The parameter $\lambda > 0$ appearing in the phase field equation is assumed small and is related to the width of the diffuse interface. Further, $P(\phi) = 8\phi^2(1-\phi)^2$ is the double-well potential, which ensures that the phase field mainly attains values (close to) 0 and 1 for small values of λ. Formally, this follows from the observation that if λ is small, the term $P'(\phi)$ dominates in (2.4a), implying that ϕ approaches one of the three equilibrium values $0, 1/2, 1$. Later we show that $1/2$ is an unstable equilibrium, from which the conclusion follows.

The reaction rate $f(u)$ and diffusion parameter γ are the same as those in the sharp-interface formulation. Note that due to the $4\phi(1-\phi)$ factor, the reaction term is nonzero only in the diffuse transition zone between the two phases, and this factor ensures that ϕ stays between 0 and 1. Note that in sharp-interface models, further dissolution after all mineral is dissolved is usually avoided by using a multivalued dissolution rate based on a Heaviside graph (see [25, 46]), which complicates the analysis and the development of numerical schemes (see [3, 27]). This is superfluous for the phase field formulation proposed here because in the absence of mineral, only the water phase is present, implying $\phi \equiv 1$, and therefore no dissolution can take place.

2.2.2. Comments on the flow equations (2.4b) and (2.4c). The flow equations are now also defined in the mineral phase. To ensure that flow only occurs in the fluid and not in the mineral, some modifications have been made. First, the flow velocity $\mathbf{q}$ and pressure gradient ∇p have become $\phi\mathbf{q}$ and $\phi\nabla p$. This leaves the flow equations unchanged in the fluid phase when $\phi = 1$, whereas these quantities are vanishing in the mineral phase where $\phi = 0$.

Second, the term $g(\phi, \lambda)\mathbf{q}$ is added. Here, $g(\phi, \lambda)$ is decreasing in the first argument, surjective, and twice differentiable and fulfills $g(1, \lambda) = 0$ and $g(0, \lambda) > 0$. This way, $\mathbf{q} = \mathbf{0}$ is the only possible solution when $\phi = 0$ (also see assumption A.4 in [22]). Moreover, this term must also ensure that the velocities in the diffuse transition zone between $\phi = 0$ and $\phi = 1$ are low, and therefore it works as an interpolation function for velocities in this zone. In [8], dealing with a similar model for melting and solidification, an artificial friction term is introduced to ensure the desired behavior for $\phi\mathbf{q}$ inside the diffuse interface. Using the current notation, their friction term would correspond to $g(\phi, \lambda) = \frac{K(1-\phi)^2\phi}{\lambda^2}$ for some constant K [8]. However, as will be explained in Remark 3.1, a term of $O(\lambda^{-2})$ would restrict the phase field model from approaching the sharp-interface model when $\lambda \searrow 0$, and therefore it is not adopted here.

A similar idea is adopted in [22], focusing on shape optimization, where the term $g(\phi, \lambda) = \frac{K}{\sqrt{\lambda}} \frac{(1-\phi)n}{\phi + n}$ is applied. The constant $n > 0$ determines the shape of the

function g. More precisely, a larger value of n leads to a function that is close to an affine one, behaving as $(1-\phi)$. In [22], $n = 10$ was found to work better regarding numerical results. Inspired by [22], here we let $g(\phi, \lambda) = \frac{K}{\lambda}\frac{(1-\phi)n}{\phi+n}$ with $n = 10$. Later we will see that this gives good numerical results for the present model too. However, any function g fulfilling the requirements listed previously can be adopted, the specific choice being based on the impact on the numerical behavior.

Finally, the term $\frac{1}{2}\rho_f \mathbf{q}\partial_t\phi$ added to (2.4c) accounts for the combined flow with accumulation of the phase field variable to ensure conservation of kinetic energy when there is precipitation. Note that the two time derivatives can be combined and rewritten as $\rho_f\sqrt{\phi}\partial_t(\sqrt{\phi}\mathbf{q})$, a formulation used in, e.g., [9].

2.2.3. Comments on the ion transport equation (2.4d). Compared to [38], the only difference appearing in the ion transport equation (2.4d) is in the presence of the convective term. Note that the time derivative can be rewritten as $\partial_t(\phi u + (1-\phi)u^*)$. This is nothing but the derivative of the phase field weighted convex combination of ion concentrations u (in the fluid phase) and the mineral concentration u^* (in the mineral phase). Recalling that in the mineral phase there is no diffusive or convective transport, we see that (2.4d) represents the total mass balance of the species.

2.2.4. Decreasing energy of the phase field formulation. The energy associated with the model (2.4) is given by

$$E = \frac{1}{2}\rho_f\phi\mathbf{q}^2 + \gamma\lambda^{-1}P(\phi) + \frac{1}{2}\gamma\lambda|\nabla\phi|^2 + \phi F(u)$$

and is the sum of the kinetic energy, the free energy of the phase field, and the energy of the ions. The function $F(u)$ is defined implicitly as a solution to the equation

$$\frac{1}{u^*}f(u) = F(u) - F'(u)u + F'(u)u^*.$$

As $f(u)$ is increasing with u, $F(u)$ is convex for $u < u^*$. Differentiating the above, we get that

$$\partial_t(\phi F(u)) = F'(u)\partial_t\big(\phi(u-u^*)\big) + \frac{1}{u^*}f(u)\partial_t\phi.$$

When considering (2.4) on a bounded domain Ω with no-slip boundary conditions for $\mathbf{q}$ and zero Neumann boundary conditions for ϕ and u at the boundary $\partial\Omega$, one gets

$$\frac{\mathrm{d}}{\mathrm{d}t}\int_\Omega E d\mathbf{x} = \int_\Omega \Big[-\mu_f\nabla(\phi\mathbf{q}) : \nabla(\phi\mathbf{q}) - g(\phi,\lambda)\mathbf{q}^2 - D\phi F''(u)|\nabla u|^2 \\ - \lambda^{-1}\Big(\nu - \frac{1}{u^*}f(u)\Big)\Big(\nu - 4\phi(1-\phi)\frac{1}{u^*}f(u)\Big)\Big] d\mathbf{x},$$

where $\nu = \gamma\lambda\nabla^2\phi - \gamma\lambda^{-1}P'(\phi)$. The first three terms on the right-hand side describe energy dissipation due to viscosity, friction close to the mineral, and diffusion of ions. The fourth term might be positive and thus lead to an increasing energy. This will be the case if curvature effects (see (2.2a)) counteract the ion reaction. However, for fixed λ, we get a bounded energy growth as in [38]. Note that the increasing energy is possible due to the factor $4\phi(1-\phi)$ in the reactive term in (2.4a). Using a multivalued Heaviside graph for the dissolution rate instead of the $4\phi(1-\phi)$ factor, as commented on in subsection 2.2.1, would result in a model with decreasing energy,

while a regularized Heaviside graph would not. To limit the values of ϕ between 0 and 1 and to ease the following analysis and numerical implementation, we choose to keep the $4\phi(1-\phi)$ factor and not use a Heaviside graph.

2.3. Regularized phase field formulation. The model (2.4) is formulated in the full domain Ω. In doing so, we include the term $g(\phi,\lambda)\mathbf{q}$ to ensure that $\mathbf{q}=\mathbf{0}$ in the mineral phase. Observe that the ion concentration u and the fluid pressure p are also defined in the region occupied by the mineral in the sharp-interface formulation. For u, a possible extension in the mineral domain is u^*, but this may lead to difficulties related to the regularity of u in the transition from the phase field model to the sharp-interface one, when $\lambda \to 0$. Moreover, there is no indication about how to extend p in the mineral domain. At the same time, the model in (2.4) does not provide any information about what values u and p should attain in the mineral domain. Although the structure of the phase field equation (2.4a) ensures that ϕ will never reach 0 (or 1), unless initialized or if appearing on the boundary $\partial\Omega$, ϕ can become arbitrarily close to 0 (and 1). From a numerical point of view, this can lead to a badly conditioned discretization, as the last two equations in (2.4) are close to degenerate whenever $\phi \searrow 0$ and cannot be used to determine u and p in the mineral. To avoid this, we regularize the model by adding a small, nondimensional $\delta > 0$ to the phase field ϕ in the mass, momentum, and solute conservation equations. The regularized model becomes

$$\lambda^2\partial_t\phi + \gamma P'(\phi) = \gamma\lambda^2\nabla^2\phi - 4\lambda\phi(1-\phi)\frac{1}{u^*}f(u), \tag{2.5a}$$

$$\nabla\cdot\big((\phi+\delta)\mathbf{q}\big) = 0, \tag{2.5b}$$

$$\begin{aligned}\rho_f\partial_t\big((\phi+\delta)\mathbf{q}\big) + \rho_f\nabla\cdot\big((\phi+\delta)\mathbf{q}\otimes\mathbf{q}\big) &= -(\phi+\delta)\nabla p\\ &\quad +\mu_f(\phi+\delta)\nabla^2\big((\phi+\delta)\mathbf{q}\big) - g(\phi,\lambda)\mathbf{q} + \frac{1}{2}\rho_f\mathbf{q}\partial_t\phi,\end{aligned} \tag{2.5c}$$

$$\partial_t\big((\phi+\delta)(u-u^*)\big) + \nabla\cdot\big((\phi+\delta)\mathbf{q}u\big) = D\nabla\cdot\big((\phi+\delta)\nabla u\big). \tag{2.5d}$$

Note that this regularization is only needed to facilitate the numerical discretization. For completeness, we use it also in the analysis given below.

Remark 2.1. The results for decreasing and limited growth of the free energy discussed in subsection 2.2.4 are also valid for the regularized formulation. To see this, one only needs to replace ϕ by $\phi+\delta$ in the terms associated with the kinetic energy and the energy of the ions.

3. The sharp-interface limit of the phase field formulation. As stated before, the phase field model can be seen as an approximation of the sharp-interface model, defined in the entire domain and where the free boundary is replaced by a diffuse interface region. To justify this, we investigate the limit of the phase field model in (2.5) as λ, the width of the diffuse transition zone, approaches zero and show that this limit is exactly the model in subsection 2.1. We follow the ideas of [14] and distinguish between the behaviors of the solution close to the interface and far away from it. To this aim we first let L be a typical length in the model and introduce the new, dimensionless parameter $\xi = \lambda/L$ related to thickness of the diffuse interface region. We investigate the behavior of the solution as $\xi \searrow 0$ by expanding the unknowns in terms of ξ and equating terms of similar order. This is done in two different ways, close to the diffuse interface (the inner expansions) and away from it (the outer expansions), which are connected by applying matching conditions in the transition region where both expansions are valid.

Before proceeding we mention that for the phase field equation, the steps are the same as in [38] and therefore are only shown briefly. Throughout this matched asymptotic analysis we take the regularization parameter as $\delta = \xi$. This choice is made for convenience as δ is not needed in the sharp-interface model. In subsequent sections, δ and ξ (or λ) can be chosen independently.

3.1. The two expansions and matching conditions. Away from the interface, we consider the *outer expansion* of ϕ, u, p, and $\mathbf{q}$. For ϕ this reads as

$$\phi^{\text{out}}(t,\mathbf{x}) = \phi_0^{\text{out}}(t,\mathbf{x}) + \xi\phi_1^{\text{out}}(t,\mathbf{x}) + \xi^2\phi_2^{\text{out}}(t,\mathbf{x}) + \cdots \tag{3.1}$$

and similarly for the other unknowns.

For the *inner expansion*, valid near the diffuse interface, we switch to local coordinates. More precisely, we let $\Gamma(t)$ denote the set of points $\mathbf{y}_\xi \in \Omega$ along which $\phi(\mathbf{y}_\xi, t) = 1/2$. Observe that these points depend on t, and on ξ as the model depends on $\lambda = L\xi$. With $\mathbf{s}$ being the parameterization along $\Gamma_\xi(t)$ ($\mathbf{s}$ being a scalar in the two-dimensional case) and $\mathbf{n}_\xi$ the normal vector at $\Gamma_\xi(t)$ pointing into the mineral, one can define r, the signed distance from a point $\mathbf{x}$ near $\Gamma_\xi(t)$ to this interface. Clearly, r depends on $\mathbf{x}$ and t and is positive in the mineral region. One gets

$$\mathbf{x} = \mathbf{y}_\xi(t,\mathbf{s}) + r\mathbf{n}_\xi(t,\mathbf{s}), \tag{3.2}$$

as presented in Figure 1. It can be shown (see [14]) that

$$|\nabla r| = 1, \quad \nabla r \cdot \nabla s_i = 0, \quad \partial_t r = -v_n, \quad \nabla^2 r = \frac{\kappa + 2\Pi r}{1 + \kappa r + \Pi r^2},$$

where κ and Π are the mean and Gaussian curvatures of the interface. Further, the point $\mathbf{y}_\xi$ has the expansion $\mathbf{y}_\xi = \mathbf{y}_0 + \xi\mathbf{y}_1 + \cdots$, where $\mathbf{y}_0$ is a point on the interface $\Gamma_0^{\text{out}}(t)$ defined through $\phi_0^{\text{out}} = 1/2$, and similarly $\mathbf{n}_\xi = \mathbf{n}_0 + \xi\gamma_1\mathbf{n}_1 + O(\xi^2)$, where $\mathbf{n}_0$ is the normal vector of $\Gamma_0^{\text{out}}(t)$.

With $z = r/\xi$ and in terms of z and $\mathbf{s}$, we consider the *inner expansions*

$$\phi^{\text{in}}(t,\mathbf{x}) = \phi_0^{\text{in}}(t,z,\mathbf{s}) + \xi\phi_1^{\text{in}}(t,z,\mathbf{s}) + \xi^2\phi_2^{\text{in}}(t,z,\mathbf{s}) + \cdots \tag{3.3}$$

and similarly for the other unknowns. In the curvilinear coordinates (3.2), by the scaling of the z variable, the derivatives are rewritten as follows. For a generic variable v or $\mathbf{v}$, we obtain [14]

$$\begin{aligned}
\partial_t v &= -\xi^{-1}v_{n,0}\partial_z v^{\text{in}} + (\partial_t + \partial_t s \cdot \nabla_{\mathbf{s}})v^{\text{in}} + O(\xi),\\
\nabla_x v &= \xi^{-1}\partial_z v^{\text{in}}\mathbf{n}_0 + \nabla_\Gamma v^{\text{in}} + O(\xi),\\
\nabla_x \cdot \mathbf{v} &= \xi^{-1}\partial_z \mathbf{v}^{\text{in}} \cdot \mathbf{n}_0 + \nabla_\Gamma \cdot \mathbf{v}^{\text{in}} + O(\xi),\\
\nabla_x^2 v &= \xi^{-2}\partial_{zz} v + \xi^{-1}\kappa_0\partial_z v + O(1),
\end{aligned}$$

where we have used $\nabla_x^2 r = \kappa_0 + O(\xi)$ as the lowest order mean curvature and $v_n = v_{n,0} + O(\xi)$. Here, κ_0 and $v_{n,0}$ are the curvature and normal velocity of the interface $\Gamma_0^{\text{out}}(t)$. Further, in the last equality the properties $|\nabla r| = 1$ and $\nabla r \cdot \nabla s_i = 0$ have been used.

For the outer expansion and a fixed t and $\mathbf{s}$, we let $\mathbf{y}_{1/2\pm}$ denote the limit $r \searrow 0$ (i.e., from the mineral side), respectively $r \nearrow 0$ (from the fluid side), of $\mathbf{x}$ rewritten in terms of the local coordinates in (3.2). We associate the corresponding limit values of the outer expansion with the ones for the inner expansion, obtained when $z \to \pm\infty$.

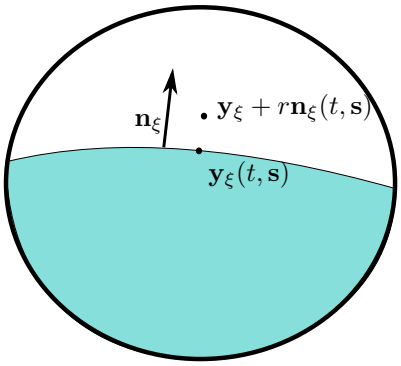

FIG. 1. *Local coordinates near the interface.*

More precisely, we assume that the two expansions of the phase field ϕ fulfill the following matching conditions [14]:

$$\lim_{z\to\pm\infty} \phi_0^{\text{in}}(t,z,\mathbf{s}) = \phi_0^{\text{out}}(t,\mathbf{y}_{1/2\pm}), \tag{3.4a}$$

$$\lim_{z\to\pm\infty} \partial_z\phi_0^{\text{in}}(t,z,\mathbf{s}) = 0, \tag{3.4b}$$

$$\lim_{z\to\pm\infty} \left(\phi_1^{\text{in}}(t,z,\mathbf{s}) - (z+y_1)\nabla\phi_0^{\text{out}}(t,\mathbf{y}_{1/2\pm})\cdot\mathbf{n}_0\right) = \phi_1^{\text{out}}(t,\mathbf{y}_{1/2\pm}), \tag{3.4c}$$

$$\lim_{z\to\pm\infty} \partial_z\phi_1^{\text{in}}(t,z,\mathbf{s}) = \nabla\phi_0^{\text{out}}(t,\mathbf{y}_{1/2\pm})\cdot\mathbf{n}_0, \tag{3.4d}$$

and similarly for the other unknowns.

3.2. Outer expansions. Following the steps in [38], we substitute the outer expansion (3.1) for ϕ into the phase field equation (2.5a). For the $O(1)$ term, which is the leading order, one obtains

$$P'(\phi_0^{\text{out}}) = 0.$$

This equation has three solutions: $\phi_0^{\text{out}} = 0,\ 1/2$, and 1. Using the formal argument in [49], the first and last solutions are stable since $P''(0)$ and $P''(1)$ are positive, whereas $\phi_0^{\text{out}} = 1/2$ is unstable since $P''(1/2) < 0$. In view of this, we see that in the limit $\xi \to 0$, one obtains the solutions $\phi_0^{\text{out}} = 0$ and $\phi_0^{\text{out}} = 1$, and we let $\Omega_0^f(t)$ and $\Omega_0^m(t)$ be the (time-dependent) subdomains of Ω where ϕ_0^{out} is 1 and 0, respectively.

Using the outer expansions in the flow equations (2.5b) and (2.5c) and the ion conservation (2.5d), it is straightforward to show that the original sharp-interface model equations (2.1) are recovered for the points in $\Omega_0^f(t)$. Moreover, for the flow equations, one also obtains $\mathbf{q}_0^{\text{out}} = \mathbf{0}$ in $\Omega_0^m(t)$.

3.3. Inner expansions. We now apply the inner expansions and the matching conditions to the phase field model to recover the boundary conditions at the evolving interface.

3.3.1. Phase field equation. For the phase field equation (2.5a) we follow the steps in [38] and obtain that the dominating $O(1)$ terms satisfy

$$P'(\phi_0^{\text{in}}) = L^2\partial_z^2\phi_0^{\text{in}}. \tag{3.5}$$

Due to (3.4), one has $\lim_{z\to-\infty} = \phi_0^{\text{in}}(t,z,\mathbf{s}) = 1$ and $\lim_{z\to\infty}\phi_0^{\text{in}}(t,z,\mathbf{s}) = 0$. Further, $\phi_0^{\text{in}}(t,0,\mathbf{s}) = 0.5$, as this should define the moving interface when $\xi \to 0$. Hence, multiplying (3.5) by $\partial_z^2\phi_0^{\text{in}}$, integrating the result in z, and using the matching conditions fulfilled by ϕ_0^{in} and the specific form of $P(\phi)$, one gets

$$\partial_z\phi_0^{\text{in}} = -\frac{4}{L}\phi_0^{\text{in}}(1-\phi_0^{\text{in}}). \tag{3.6}$$

Since $\phi_0^{\text{in}}(t,0,\mathbf{s}) = 1/2$, the solution is

$$\phi_0^{\text{in}}(t,z,\mathbf{s}) = \phi_0^{\text{in}}(z) = \frac{1}{1+e^{4z/L}} = \frac{1}{2}\Big(1+\tanh\Big(\frac{2z}{L}\Big)\Big). \tag{3.7}$$

For the $O(\xi)$ terms, one obtains

$$\big(P''(\phi_0^{\text{in}}) - L^2\partial_z^2\big)\phi_1^{\text{in}} = (L^2 v_{n,0} + L^2\gamma\kappa_0)\partial_z\phi_0^{\text{in}} - 4L\phi_0^{\text{in}}(1-\phi_0^{\text{in}})\frac{1}{u^*}f(u_0^{\text{in}}).$$

We view the left-hand side as an operator $\mathcal{L}$ depending on ϕ_0^{in} and applied to ϕ_1^{in}. As $\mathcal{L}$ is a Fredholm operator of index zero, the above equation has a solution if and only if the right-hand side, denoted by $A(\phi_0^{\text{in}})$, is orthogonal to the kernel of $\mathcal{L}$. As follows from (3.5), $\partial_z\phi_0^{\text{in}}$ lies in the kernel of $\mathcal{L}$. Since $v_{n,0}$, κ_0, and u_0^{in} are independent of z (the latter will be shown in the following section), the solvability condition implies

$$\begin{aligned}
0 &= \int_{-\infty}^{\infty} A(\phi_0^{\text{in}})\partial_z\phi_0^{\text{in}}dz \\
&= L^2(v_{n,0}+\gamma\kappa_0)\int_{-\infty}^{\infty}(\partial_z\phi_0^{\text{in}})^2dz - 4L\frac{1}{u^*}f(u_0^{\text{in}})\int_{-\infty}^{\infty}\phi_0^{\text{in}}(1-\phi_0^{\text{in}})\partial_z\phi_0^{\text{in}}dz \\
&= \frac{2}{3}L\Big(v_{n,0}+\gamma\kappa_0+\frac{1}{u^*}f(u_0^{\text{in}})\Big).
\end{aligned}$$

From this, by applying matching conditions for u at the moving interface, we obtain the condition

$$v_{n,0} = -\gamma\kappa_0 - \frac{1}{u^*}f(u_0^{\text{out}}(t,\mathbf{y}_{1/2-})),$$

which is the first boundary condition (2.2a) at the moving interface.

3.3.2. Mass conservation equation. The dominating $O(\xi^{-1})$ term arising from inserting the inner expansions into (2.5b) is

$$\partial_z(\phi_0^{\text{in}}\mathbf{q}_0^{\text{in}})\cdot\mathbf{n}_0 = 0. \tag{3.8}$$

By integrating with respect to z and using matching conditions, we obtain

$$\mathbf{q}_0^{\text{out}}(t,\mathbf{y}_{1/2-})\cdot\mathbf{n}_0 = 0.$$

In other words, the normal component of the velocity is zero at the moving interface. To conclude the same for the tangential component, we consider the momentum conservation equation.

3.3.3. Momentum conservation equation. The dominating $O(\xi^{-2})$ term in the momentum equation (2.5c) is

$$\mu_f\phi_0^{\text{in}}\partial_z^2(\phi_0^{\text{in}}\mathbf{q}_0^{\text{in}}) = \mathbf{0}.$$

Integrating with respect to z and using matching conditions results in

$$\mathbf{q}_0^{\text{out}}(t, \mathbf{y}_{1/2-}) = \mathbf{0},$$

which is the second boundary condition (2.2b) at the moving interface.

Remark 3.1. Note that choosing $g(\phi, \lambda) = \frac{K\phi(1-\phi)^2}{\lambda^2}$ as in [8] would lead to the dominating $O(\xi^{-2})$ terms being

$$\mu_f \phi_0^{\text{in}} \partial_z^2(\phi_0^{\text{in}} \mathbf{q}_0^{\text{in}}) = K\phi_0^{\text{in}}(1-\phi_0^{\text{in}})^2 \mathbf{q}_0^{\text{in}}.$$

Although μ_f and K are constants, and ϕ_0^{in} is known through (3.7), solving this equation for $\mathbf{q}_0^{\text{in}}$ is not straightforward, and therefore it is unclear whether $\mathbf{q}_0^{\text{out}}(t, \mathbf{y}_{1/2-}) = \mathbf{0}$ is recovered in this case.

3.3.4. Ion conservation equation. The dominating $O(\xi^{-2})$ term obtained by inserting the inner expansions into (2.5d) is

$$\partial_z(\phi_0^{\text{in}} \partial_z u_0^{\text{in}}) = 0.$$

Integrating with respect to z and using matching conditions and the fact that $\phi_0^{\text{in}} > 0$, we obtain

$$\partial_z u_0^{\text{in}} = 0,$$

and hence $u_0^{\text{in}} = u_0^{\text{in}}(t, \mathbf{s})$ as mentioned in the previous section.

Taking advantage of $\partial_z u_0^{\text{in}} = 0$ and (3.8), the $O(\xi^{-1})$ terms satisfy

$$-v_{n,0}(u_0^{\text{in}} - u^*)\partial_z \phi_0^{\text{in}} = D\partial_z(\phi_0^{\text{in}} \partial_z u_1^{\text{in}}).$$

Integrating with respect to z from $-\infty$ to $+\infty$ and applying matching conditions lead to

$$v_{n,0}(u_0^{\text{out}}(t, \mathbf{y}_{1/2-}) - u^*) = -D\nabla u_0^{\text{out}}(t, \mathbf{y}_{1/2-}) \cdot \mathbf{n}_0,$$

which is the third boundary condition (2.2c) at the moving interface.

4. Numerical behavior of the phase field model. We consider two numerical examples showing the applicability and the potential of the model (2.5) by studying the dissolution of a mineral crystal located in a channel and subject to a flow field. The first example is from the benchmark study [33], and we assess how the phase field model (2.5) behaves for a specific case compared to the results in the benchmark study. In the second example, we make a qualitative assessment of how the mineral dissolution process is affected by the strength of the flow field, inspired by the sharp-interface simulations in [34].

4.1. Dissolution of a calcite crystal. We consider the benchmark problem II from [33]. Here, calcite dissolves through the chemical reaction

$$\text{CaCO}_3(s) + \text{H}^+(l) \to \text{Ca}^{2+}(l) + \text{HCO}_3^-(l).$$

Since H^+ is needed for calcite to dissolve, we model this as a one-way reaction, where (2.5d) is replaced by

$$\partial_t\big((\phi+\delta)(u_{H^+} + u^*)\big) + \nabla \cdot \big((\phi+\delta)\mathbf{q}u_{H^+}\big) = D\nabla \cdot \big((\phi+\delta)\nabla u_{H^+}\big), \tag{4.1}$$

and use the simple, linear reaction rate

$$f(u_{H^+}) = -ku_{H^+} \tag{4.2}$$

in (2.5a). This means there is no precipitation, and the dissolution rate increases with larger access to H^+. Note the change in sign in the time derivative in (4.1) compared to (2.5d). This occurs because H^+ is consumed, not produced, for calcite to dissolve. Writing the time derivative as $\partial_t\big(\phi u_{H^+} - (1-\phi)u^*\big)$ as in subsection 2.2.3 shows that we are conserving the difference between H^+ and the mineral, reflecting that as one calcite molecule dissolves, one H^+ atom is consumed. We do not model the concentrations of the solutes Ca^{2+} and HCO_3^- as they do not affect the reaction rate.

We follow the same setup as in [33] by considering a two-dimensional channel of length 1 mm and width 0.5 mm, where a circular calcite crystal of initial radius 0.1 mm is centered in (0.5, 0.25) mm. A uniform flow field of given velocity $q_{\text{in}} = 0.0012$ m/s is applied at $x = 0$ mm. Initially and at the inlet a concentration of $u_{H^+} = 10$ mol/m^3 is applied. The top and bottom of the channel are no-slip boundaries, while fluid can leave through the outlet at $x = 1$ mm. We refer the reader to Table 1 for all specified parameters for model (2.5a)–(2.5c) and (4.1). All parameters not related to the phase field are taken from [33].

TABLE 1
Parameters corresponding to benchmark II *in* [33] *and phase field parameters.*

Parameter	Symbol	Value	Units
Fluid density	ρ_f	10^3	kg m^{-3}
Fluid viscosity	μ_f	10^{-3}	kg m^{-1}s^{-1}
Diffusion coefficient	D	10^{-9}	m^{2}s^{-1}
Inlet velocity	q_{in}	0.0012	m s^{-1}
Reaction rate constant in (4.2)	k	8.9×10^{-3}	mol m^{-2}s^{-1}
Inlet and initial concentration	u_{H^+}	10	mol m^{-3}
Calcite molar density	u^*	27100	mol m^{-3}
Phase field diffuse interface width	λ	2.5×10^{-5}	m
Phase field interface diffusivity	γ	2.8×10^{-14}	m^2 s^{-1}
Phase field regularization	δ	10^{-6}	-
Phase field flow interpolation; $g(\phi,\lambda) = \frac{10K(1-\phi)}{\lambda(\phi+10)}$	K	25	kg m^{-2} s^{-1}

The model equations are discretized using a control volume method on a uniform, rectangular staggered grid of 200×200 grid cells. The phase field, pressure, and solute are defined in the centers of the control volumes, while the velocity is defined at the center of the edges. Convective fluxes are approximated by an upstream approximation, and diffusive fluxes are discretized using a two-point approximation. The model is discretized in time using the backward Euler scheme with a constant time-step size $\Delta t = 1.35$ s until the end time $t = 2700$ s $= 45$ min. The resulting nonlinear systems of equations are solved using Newton iterations in each time step, with the previous time step as an initial guess.

Figure 2 shows the shape of the calcite crystal initially and after 15, 30, and 45 minutes. The shapes are shown by plotting the $\phi = 0.5$ isolines of the phase field. The initially circular calcite crystal dissolves unevenly due to the accessibility of H^+ varying with the flow around the crystal. Since the flow takes place from left to right, the dissolution is strongest at the left part of the calcite crystal and reduces while moving to the right part of the crystal. Comparing this to the corresponding Figure 8 in [33], we see the same qualitative change in shape. The crystal dissolves slightly faster in our approach compared to [33], which could be due to the nonconservative property of the Allen–Cahn equation.

4.2. Effect of flow field strength on dissolution. We consider a qualitative comparison with respect to how mineral dissolves when located in flow fields of

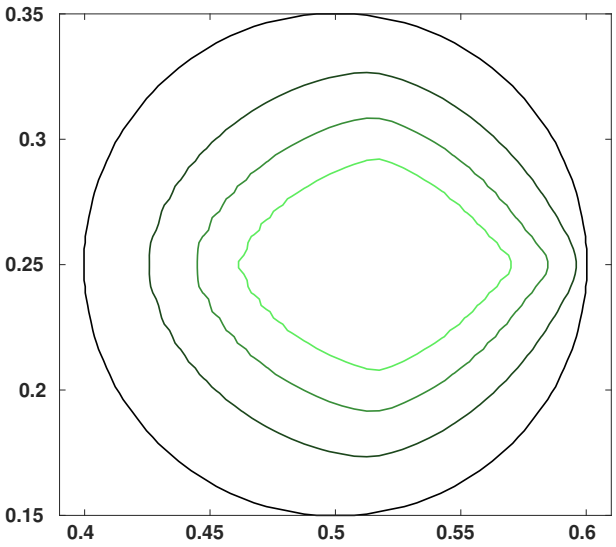

FIG. 2. *The mineral shape while dissolving (zoomed-in view of the channel where the calcite is present initially). The evolution of the calcite boundary at* $t = 0$, 15 *min,* 30 *min, and* 45 *min (from the outermost curve to the innermost one). The axis scales are in mm.*

different strengths, inspired by the setup in [34, sect. 3.1]. As in the previous test, we consider a channel of length 1 mm and width 0.5 mm, with an initially circular mineral located in $(0.5, 0.25)$ mm having radius 0.1 mm. At $x = 0$, a uniform flow field of a given velocity is applied and the fluid can flow out at $x = 1$, while the top and bottom are no-slip boundaries. We now use the original model (2.5) and reaction rate (2.3). To trigger dissolution of the mineral, we apply an equilibrium concentration $u_{\text{eq}} = 0.5$ mol/m^3, and for the solute we use an initial concentration of u_{eq} and a Dirichlet boundary condition at the inlet of $u_{\text{eq}}/2$. The Péclet and Damköhler numbers are defined as

$$\text{Pe} = \frac{Lq_{\text{in}}}{D}, \quad \text{Da} = \frac{k}{u_{\text{eq}} q_{\text{in}}},$$

where $D = 5 \times 10^{-9}$ is the diffusivity of the solute, $k = 1.9 \times 10^{-5}$ is the reaction constant, and L is the length of the channel. By varying q_{in} among (a) 1.2×10^{-5} m/s, (b) 1.2×10^{-4} m/s, (c) 1.2×10^{-3} m/s, and (d) 0.012 m/s, we consider the four Péclet and Damköhler numbers given in Table 2, which are the same cases applied in [34]. We use a mineral concentration of $u^* = 1$ mol/m^3. This is an artificially low value of a mineral density but causes the mineral to change shape faster as it dissolves. For the phase field, we use the same parameters as in Table 1.

TABLE 2
Nondimensional numbers in the four simulations.

Simulation	(a)	(b)	(c)	(d)
Péclet number	2.4	24	240	2400
Damköhler number	3.173	0.317	0.032	0.003

The model (2.5) is discretized using the same control volume method as before using a uniform, rectangular staggered grid of 200×200 grid cells. The model is time stepped using backward Euler with a constant time-step size $\Delta t = \Delta y / q_{\text{in}}$, and the nonlinear systems of equations are solved using Newton iterations in each time step, with the previous time step as an initial guess.

The four simulations are carried out until the mineral is dissolved completely. Figure 3 shows the isolines $\phi = 0.5$ at different time steps to indicate the shape of the mineral as it dissolves. Although we consider a different chemical system from that in [34], we see how the later isolines go from being circular for low velocities to more elongated at larger velocities as in [34, Figure 2]. For low velocities, the reaction rate is quite similar for the entire mineral surface, although with an increase at the front where lower solute concentrations are first met. At larger velocity, dissolution is faster on the sides as dissolved solute is more efficiently transported away, triggering further dissolution. The mineral generally dissolves faster when the Péclet number increases, although the same reaction rate has been used. This is caused by the dissolving mineral creating a local increase in the solute concentration, which is transported away more quickly when the flow velocity is large. We see how the interplay between velocity and diffusion gives the different shapes of the mineral as it dissolves, and also different effective reaction rates [20].

5. Upscaling using periodic homogenization. We now consider the phase field model (2.5) to be defined in a periodic porous medium. The pore scale, where grain, mineral, and fluid-filled void space are explicitly separated, will be the microscale, and in the following we will derive a macroscale model describing the effective behavior of the system. More precisely, we consider a domain $\mathcal{D}$ containing small, periodically distributed grains, as sketched in Figure 4. In a porous medium, $\mathcal{D}$ represents the union of the void space, mineral space, and grain space, where the grains will be considered as perforations. We will refer to the union of the void space and mineral space as the pore space. The grains are impermeable to fluid, and no reactions take place there. Hence, the phase field model (2.5) is not defined in the grain space but only in the pore space of $\mathcal{D}$. The grains do not change with time, while the moving boundary between mineral and fluid, located in the pore space of $\mathcal{D}$, is still handled by the phase field equation as a diffuse interface. We assume that the mineral precipitates on the boundary of the perforations or at already existing minerals and not inside the void space. Two important assumptions are that the void space in $\mathcal{D}$ is connected and that the mineral never grows in such a way that the pore space is clogged.

The porous medium $\mathcal{D}$ contains many periodically repeating grains. This means that the phase field model (2.5) is defined on a domain of high complexity. In such cases, the averaged behavior of the system is of primary interest. In consequence we apply periodic homogenization techniques to find effective equations valid at a larger scale, where the microscale oscillations are no longer visible, but their effect is still taken into account. This is done by identifying a scale separation and applying asymptotic expansions on nondimensional versions of the model equations.

When nondimensionalizing the model (2.5), one must address the size of the appearing nondimensional numbers (e.g., Reynolds, Péclet, Cahn, and Damköhler), in particular, their internal ordering. The size of these nondimensional numbers describes which regime we consider, and in the following we will consider a regime in the range of Darcy's law [23] and where time scales for macroscale solute diffusion, advection, and reaction are approximately the same size [6]. As we will see in the following, this leads to diffusion dominating at the pore scale. Finally, we want the

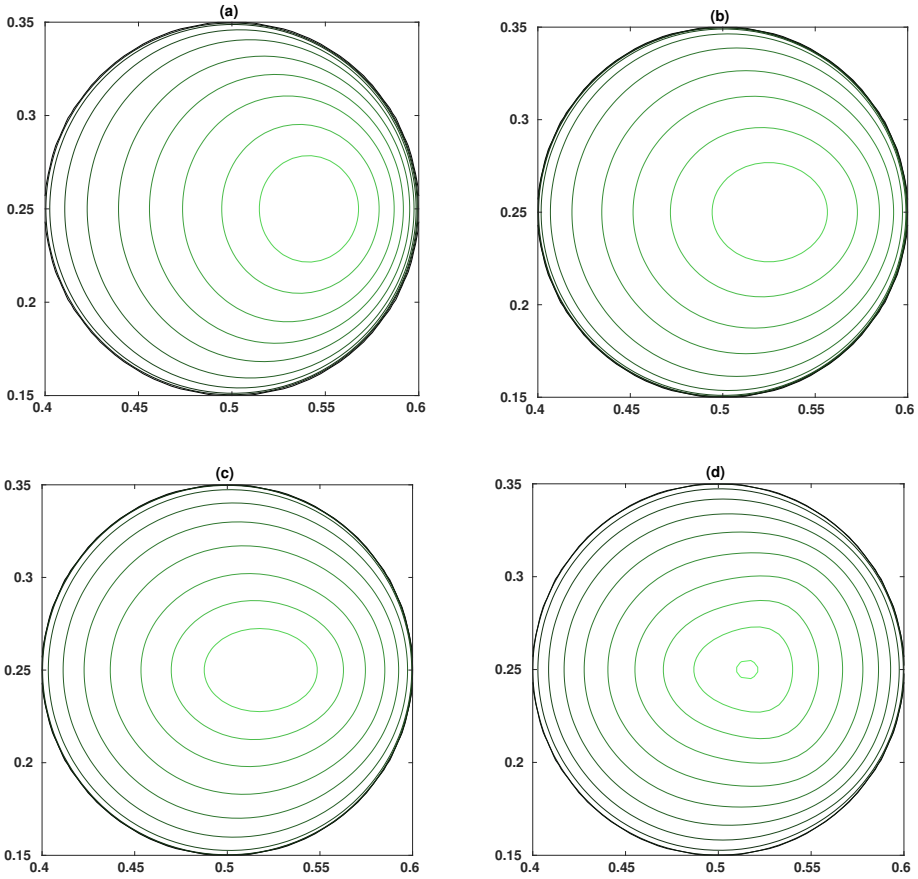

FIG. 3. *The mineral shapes while dissolving (zoomed-in view of the channel where the calcite is present initially). Black line shows initial shape, while increasingly brighter green shows the shape at later time steps. Cases* (a)–(d) *correspond to the cases in Table* 2. *The last isolines are at times* (a) $t = 3.4$ *s,* (b) $t = 1.6$ *s,* (c) $t = 1.1$ *s,* (d) $t = 0.79$ *s. The axis scales are in mm. (See online version for color.)*

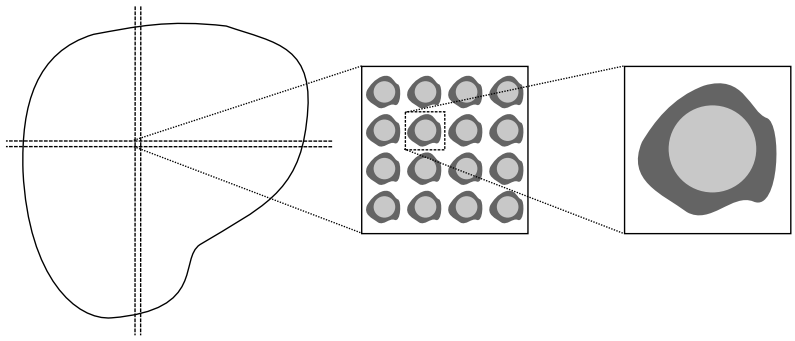

FIG. 4. *Structure of porous medium. Fluid-filled void space is marked with white, mineral is dark grey, and nonreactive grain is light grey. The pore space is the union of the void space and mineral space.*

phase field to appear as a local, microscale variable, and we will address the choices necessary to achieve this. Note that other choices for the nondimensional numbers are possible but will result in different upscaled models.

5.1. The scale separation. In the dimensional setting, we let ℓ be a typical length scale at the microscale (that is, the pore scale), e.g., the width of the rightmost box in Figure 4, and let L be a typical length scale at the macroscale, e.g., the width of the domain $\mathcal{D}$ or of the Darcy scale, as commonly made for homogenization [19, 23]. With this we define $\varepsilon = \ell/L$, reflecting the ratio between the micro- and macroscales and hence giving us the scale separation. We assume that ℓ is much smaller than L, and hence ε is a small number. We mention that [46, Remark 1.2] discusses a different definition of the scale separation and shows how this leads to the same nondimensional model.

In what follows we rewrite the model in nondimensional form. In doing so we introduce a local unit cell $Y = [0,1]^{\mathrm{dim}}$, as seen in Figure 5, where dim is 2 or 3, depending on spatial dimension, and we let the local variable $\mathbf{y} \in (0,1)^{\mathrm{dim}}$ describe points within Y. The local cell consists of the fluid part F and mineral part M, and the grain part G is as sketched in Figure 5. Hence, locally the phase field model is defined in the pore space $P = F \cup M$, while G defines the perforation. The boundary Γ_P defines the (stationary) internal boundary between the perforation and the domain for the phase field model. The boundary ∂Y denotes the outer boundary of the unit cell Y. At this boundary we will later apply periodic boundary conditions, allowing us to decouple the unit cells from one another. However, when referring to internal boundaries, the boundary Γ_P is meant.

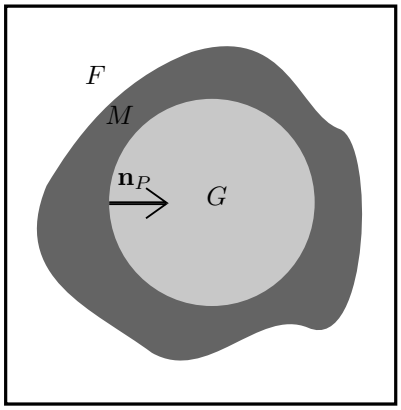

FIG. 5. *Local pore $Y = [0,1]^d$. The fluid part (white) is F, mineral part (dark grey) is M, and grain part (light grey) is G, along with a normal vector $\mathbf{n}_P$ at the internal boundary Γ_P. The outer boundary of the local pore, ∂Y, is marked with black.*

To distinguish between the two scales in the model, we use $\mathbf{x}$ as the variable at the macroscale, which is then connected to the local, microscale variable $\mathbf{y}$ through $\mathbf{y} = \varepsilon^{-1}\mathbf{x}$. This can be interpreted as $\mathbf{x}$ only seeing the macroscale behavior, while the zoomed-in $\mathbf{y}$ sees the microscale rapid changes in a single cell. Hence for each macroscale point $\mathbf{x}$, we can identify a unit cell, with its own local variable $\mathbf{y}$.

With this we have that the perforated domain of the phase field model is the union of all local pores P, scaled by ε. This means that the domain depends on ε and

can be written as

$$\Omega^\varepsilon = \cup_{w\in W_\mathcal{D}}\{\varepsilon(w+P)\},$$

where $W_\mathcal{D}$ is a subset of $\mathbb{Z}^{\dim}$ satisfying $\mathcal{D} = \cup_{w\in W_\mathcal{D}}\{\varepsilon(w+Y)\}$, which is the complete (nonperforated) medium domain seen to the left in Figure 4. We use ε as a superscript to indicate dependence on ε. The union of all internal boundaries Γ_P is denoted by

$$\Gamma^\varepsilon = \cup_{w\in W_\mathcal{D}}\{\varepsilon(w+\Gamma_P)\}.$$

5.2. Nondimensional model equations. To identify which terms are dominating in the model and hence are important for the upscaling, we first nondimensionalize the model equations (2.5). The assumptions made below on the typical flow rate, viscosity, and pressure difference ensure that we are in the range of Darcy's law, which means that at the macroscale the conservation of momentum equation (2.5c) becomes a Darcy-like law. Also, we ensure that the diffuse interface (that is, the transition between mineral and fluid) stays within a local pore. Nondimensional variables and quantities are denoted with a hat and are defined as

$$\begin{aligned}
&\hat{t} = t/t_{\text{ref}}, && \hat{\mathbf{x}} = \mathbf{x}/L, && \hat{\mathbf{y}} = \mathbf{y}/\ell, && \hat{\lambda} = \lambda/\lambda_{\text{ref}},\\
&\hat{\mathbf{q}}^\varepsilon = \mathbf{q}/q_{\text{ref}}, && \hat{u}^\varepsilon = u/u_{\text{ref}}, && \hat{p}^\varepsilon = p/p_{\text{ref}}, && \hat{u}^* = u^*/u_{\text{ref}},\\
&\hat{D} = D/D_{\text{ref}}, && \hat{\mu}_f = \mu_f/\mu_{\text{ref}}, && \hat{\rho}_f = \rho_f/\rho_{\text{ref}}, && \hat{k} = k/k_{\text{ref}},\\
& && \hat{\gamma} = \gamma/\gamma_{\text{ref}}, && \hat{K} = K/K_{\text{ref}}. &&
\end{aligned}$$

Note the superscript ε for the variables having a highly oscillatory behavior. The relations between the reference quantities are given through several nondimensional numbers. The size of these nondimensional numbers describes which regime we consider. As already mentioned, here we are interested in the regime where Darcy's law is valid and where solute advection, diffusion, and reaction time scales are about the same order of magnitude. Darcy's law is valid when fluid flow is laminar and when the pressure drop dominates the flow behavior. This corresponds to the Reynolds and Euler numbers being

$$\text{Re} = \rho_{\text{ref}} q_{\text{ref}} L/\mu_{\text{ref}} = O(\varepsilon^0), \quad \text{Eu} = p_{\text{ref}}/q_{\text{ref}}^2\rho_{\text{ref}} = O(\varepsilon^{-2}),$$

respectively. Different choices can, e.g., lead to the Forchheimer law [16]. Solute advection, diffusion, and reaction time scales are identified as $t_{\text{adv}} = L/q_{\text{ref}}$, $t_{\text{diff}} = L^2/D_{\text{ref}}$, and $t_{\text{react}} = u_{\text{ref}}\ell/k_{\text{ref}}$, respectively. These time scales are assumed to be about the same, that is, that advection, diffusion, and reaction are equally important, which corresponds to the Péclet and Damköhler numbers being

$$\text{Pe} = t_{\text{diff}}/t_{\text{adv}} = O(\varepsilon^0), \quad \text{Da} = t_{\text{adv}}/t_{\text{react}} = O(\varepsilon^0),$$

respectively. Upscaled models have also been derived for other regimes with respect to the Péclet and Damköhler numbers by employing either homogenization [4, 12, 17, 28, 32, 45] or volume averaging techniques [53, 54]. The observation time scale t_{ref} is set to be equal to t_{adv}.

For reference quantities and parameters affecting the phase field variable, we assume that the diffuse interface width is proportional to, but still smaller than, the pore size ℓ. This corresponds to the Cahn number being

$$\text{Ca} = \lambda_{\text{ref}}/L = O(\varepsilon).$$

Hence, $\hat{\lambda}$ is a small number but independent of ε. This way, the interface width is small relative to the pore size but remains a microscale quantity without approaching its sharp-interface limit as ε approaches zero. Similar choices are made in the upscaling of the phase field models found in [18, 31, 38], while an interface width that is large compared to the pore size is upscaled in [41, 42]. In the latter two papers, the phase field appears as a macroscale variable in the upscaled model. The microscale diffusive time scale of the phase field, that is, $t_{\text{diff},\gamma} = \ell^2/\gamma_{\text{ref}}$, is chosen to be comparable to the reactive time scale, but where $\hat{\gamma}$ is still allowed to be small but independent of ε (that is, $O(\varepsilon^0)$). Hence, the diffusive Damköhler number of the phase field is

$$\text{Da}_\phi = t_{\text{diff},\gamma}/t_{\text{react}} = O(\varepsilon^0).$$

This choice supports the phase field variable as a microscale variable, without affecting the sharp-interface limit as ε approaches zero. Finally, the reference value K_{ref} is chosen in relation to the other flow-related reference values to ensure low velocities in the diffuse transition zone as ε approaches zero. Interpreting K_{ref} as viscosity divided by a slip length, this corresponds to the Navier number being

$$\text{Na} = \ell_s/L = O(\varepsilon),$$

where $\ell_s = \mu_{\text{ref}}/K_{\text{ref}}$ is the associated slip length.

For readability, in the following we let the nondimensional numbers that are equal to $O(\varepsilon^k)$ be exactly equal to ε^k, but other choices for the proportionality constants are straightforward. Hence, we now have that $\text{Re} = 1$, $\text{Eu} = \varepsilon^{-2}$, etc. This corresponds to letting $\mu_{\text{ref}} = \rho_{\text{ref}} L q_{\text{ref}}$ and $p_{\text{ref}} = q_{\text{ref}}^2 \rho_{\text{ref}} L^2/\ell^2$. From the Péclet and Damköhler numbers, we get $k_{\text{ref}} = u_{\text{ref}}\ell/t_{\text{ref}}$ and $D_{\text{ref}} = L^2/t_{\text{ref}}$. With this choice of k_{ref}, the nondimensional reaction rate can be defined as $\hat{f}(\hat{u}) = \hat{k}(\hat{u}^2/\hat{u}_{\text{eq}}^2 - 1)$. $\text{Ca} = \varepsilon$ corresponds to letting $\lambda_{\text{ref}} = \ell$, and $\text{Da}_\phi = 1$ corresponds to $\gamma_{\text{ref}} = \ell^2/t_{\text{ref}}$. Finally, $\text{Na} = \varepsilon$ means that $K_{\text{ref}} = \rho_{\text{ref}} q_{\text{ref}} L/\ell$.

Table 3 summarizes the choices made in the nondimensionalization.

TABLE 3
Nondimensional quantities and their relation to the upscaling parameter ε.

Dimensionless number	Definition	Size w.r.t. ε
Scale separation	$\varepsilon = \ell/L$	ε
Reynolds number	$\text{Re} = \rho_{\text{ref}} q_{\text{ref}} L/\mu_{\text{ref}}$	ε^0
Euler number	$\text{Eu} = p_{\text{ref}}/q_{\text{ref}}^2 \rho_{\text{ref}}$	ε^{-2}
Péclet number	$\text{Pe} = L q_{\text{ref}}/D_{\text{ref}}$	ε^0
Damköhler number	$\text{Da} = k_{\text{ref}} L/u_{\text{ref}} q_{\text{ref}} \ell$	ε^0
Cahn number	$\text{Ca} = \lambda_{\text{ref}}/L$	ε
Phase field Damköhler number	$\text{Da}_\phi = k_{\text{ref}}\ell/\gamma_{\text{ref}} u_{\text{ref}}$	ε^0
Navier number	$\text{Na} = \mu_{\text{ref}}/K_{\text{ref}} L$	ε

Remark 5.1. The (nondimensional) diffuse interface width $\hat{\lambda}$, phase field diffusivity $\hat{\gamma}$, and regularization parameter δ are all small, positive numbers that are independent of ε. That means they remain fixed as $\varepsilon \to 0$ in the following section. These three numbers affect the behavior of the phase field model. In particular, $\hat{\lambda}$ is the microscale diffuse interface width, and $\hat{\gamma}$ dictates the equilibration speed of the diffuse interface, while δ assures the model is not degenerate. These numbers will be set to small numbers in the numerical examples, but they neither rely on any internal ordering nor depend on one another.

Since from now on we will only use nondimensional variables, we omit the hat on all variables. With this, the dimensionless model reads as

$$\lambda^2\partial_t\phi^\varepsilon + \gamma P'(\phi^\varepsilon) = \varepsilon^2\gamma\lambda^2\nabla^2\phi^\varepsilon - 4\lambda\phi^\varepsilon(1-\phi^\varepsilon)\frac{1}{u^*}f(u^\varepsilon) \qquad \text{in } \Omega^\varepsilon, \tag{5.1a}$$

$$\nabla\cdot\big((\phi^\varepsilon+\delta)\mathbf{q}^\varepsilon\big) = 0 \qquad \text{in } \Omega^\varepsilon, \tag{5.1b}$$

$$\begin{aligned}\varepsilon^2\rho_f\Big(\partial_t\big((\phi^\varepsilon+\delta)\mathbf{q}^\varepsilon\big) - \frac{1}{2}\mathbf{q}^\varepsilon\partial_t\phi^\varepsilon + \nabla\cdot\big((\phi^\varepsilon+\delta)\mathbf{q}^\varepsilon\otimes\mathbf{q}^\varepsilon\big)\Big) + (\phi^\varepsilon+\delta)\nabla p^\varepsilon \\ = \varepsilon^2\mu_f(\phi^\varepsilon+\delta)\nabla^2\big((\phi^\varepsilon+\delta)\mathbf{q}^\varepsilon\big) - \frac{K}{\lambda}\frac{(1-\phi^\varepsilon)n}{\phi^\varepsilon+n}\mathbf{q}^\varepsilon \qquad \text{in } \Omega^\varepsilon,\end{aligned} \tag{5.1c}$$

$$\partial_t\big((\phi^\varepsilon+\delta)(u^\varepsilon-u^*)\big) + \nabla\cdot\big((\phi^\varepsilon+\delta)\mathbf{q}^\varepsilon u^\varepsilon\big) = D\nabla\cdot\big((\phi^\varepsilon+\delta)\nabla u^\varepsilon\big) \qquad \text{in } \Omega^\varepsilon, \tag{5.1d}$$

$$\nabla\phi^\varepsilon\cdot\mathbf{n}^\varepsilon = 0 \qquad \text{on } \Gamma^\varepsilon, \tag{5.1e}$$

$$(\phi^\varepsilon+\delta)\nabla u^\varepsilon\cdot\mathbf{n}^\varepsilon = 0 \qquad \text{on } \Gamma^\varepsilon, \tag{5.1f}$$

$$\mathbf{q}^\varepsilon = \mathbf{0} \qquad \text{on } \Gamma^\varepsilon. \tag{5.1g}$$

Remark 5.2. Note that the analysis below remains unchanged if $\delta = 0$, when clogging is not considered. In other words, including an ε-independent regularization parameter δ does not affect the upscaling. The presence of $\delta > 0$ ensures that the resulting model is not degenerate, which is important for the numerical examples.

5.3. The formal asymptotic expansions. We apply the homogenization ansatz, namely we assume that the unknowns can be written as a series expansion in terms of ε with explicit dependence on the micro- and macroscale variables. For the phase field ϕ^ε this reads as

$$\phi^\varepsilon(t,\mathbf{x}) = \phi_0(t,\mathbf{x},\mathbf{y}) + \varepsilon\phi_1(t,\mathbf{x},\mathbf{y}) + \varepsilon^2\phi_2(t,\mathbf{x},\mathbf{y}) + \cdots, \tag{5.2}$$

where the functions $\phi_i(t,\mathbf{x},\mathbf{y})$ are Y-periodic in $\mathbf{y}$. Similar expansions are assumed for all dependent variables. The introduction of the microscale variable $\mathbf{y}$ is an important aspect: While the ϕ^ε needs to resolve both the microscale and macroscale behaviors, we assume that the functions in the series expansion can distinguish between slow variability through $\mathbf{x}$ and fast variability through $\mathbf{y}$. Further, the series expansion allows us to capture the dominating behavior in ϕ_0, while lower order behavior is captured through the subsequent terms. Also note that macroscale $\mathbf{x}$ is defined in the entire (nonperforated) domain $\mathcal{D}$, while $\mathbf{y}$ is defined locally in a pore P.

As $\mathbf{y}$ is a local variable behaving like $\mathbf{y} = \varepsilon^{-1}\mathbf{x}$, the spatial derivatives need to be rewritten accordingly. Hence, for a generic variable v, one has

$$\nabla v(\mathbf{x},\mathbf{y}) = \nabla_{\mathbf{x}} v(\mathbf{x},\mathbf{y}) + \frac{1}{\varepsilon}\nabla_{\mathbf{y}} v(\mathbf{x},\mathbf{y}), \tag{5.3}$$

where $\nabla_{\mathbf{x}}$ and $\nabla_{\mathbf{y}}$ are the gradients with respect to $\mathbf{x}$, respectively, $\mathbf{y}$. We insert the asymptotic expansions (5.2) and the rescaled derivatives (5.3) into the model equations (5.1), and equate terms of the same order with respect to ε to isolate the behavior of the system on different scales. In the regularized equations, the term $\phi_0+\delta$ will appear frequently, and we will use the notation $\phi_0^\delta = \phi_0+\delta$ in this case. Note that $\phi_0^\delta > 0$.

5.3.1. Phase field equation. Equating the dominating $O(1)$ terms in the phase field equation (5.1a) gives

$$\lambda^2\partial_t\phi_0 + \gamma P'(\phi_0) = \gamma\lambda^2\nabla_{\mathbf{y}}^2\phi_0 - 4\lambda\phi_0(1-\phi_0)\frac{1}{u^*}f(u_0).$$

The dominating term of the corresponding boundary condition (5.1e) gives $\nabla_{\mathbf{y}}\phi_0 \cdot \mathbf{n}_P = 0$. Observe that the above equation is similar to the original (5.1a) but involves only spatial derivatives with respect to $\mathbf{y}$. Although ϕ_0 still depends on $\mathbf{x}$, $\mathbf{x}$ only appears as a parameter, as no derivatives with respect to $\mathbf{x}$ are involved. Recalling the Y-periodicity in $\mathbf{y}$, ϕ_0 solves the following *cell problem* for the phase field:

$$\begin{aligned} \lambda^2\partial_t\phi_0 + \gamma P'(\phi_0) &= \gamma\lambda^2\nabla_{\mathbf{y}}^2\phi_0 - 4\lambda\phi_0(1-\phi_0)\frac{1}{u^*}f(u_0) && \text{in } P,\\ \nabla_{\mathbf{y}}\phi_0 \cdot \mathbf{n}_P &= 0 && \text{on } \Gamma_P,\\ \text{periodicity in } \mathbf{y} & && \text{across } \partial Y. \end{aligned} \tag{5.4}$$

These cell problems are defined for each macroscale $\mathbf{x}$, which corresponds to each pore as in Figure 5. However, the cell problems are decoupled locally due to the periodicity requirement.

5.3.2. Mass conservation equation. The dominating $O(\varepsilon^{-1})$ term in (5.1b) gives

$$\nabla_{\mathbf{y}} \cdot \left(\phi_0^\delta \mathbf{q}_0\right) = 0 \text{ in } P, \tag{5.5}$$

which will be needed in the derivation for the momentum and ion conservation equations. Next, the $O(1)$ terms provide

$$\nabla_{\mathbf{x}} \cdot \left(\phi_0^\delta \mathbf{q}_0\right) + \nabla_{\mathbf{y}} \cdot \left(\phi_0^\delta \mathbf{q}_1 + \phi_1 \mathbf{q}_0\right) = 0.$$

Integrating with respect to $\mathbf{y}$ over P and applying the Gauss theorem and the boundary conditions $\mathbf{q}_0 = \mathbf{q}_1 = \mathbf{0}$ on Γ_P, together with periodicity, one gets

$$\nabla_{\mathbf{x}} \cdot \left(\overline{\phi_0^\delta \mathbf{q}_0}\right) = 0 \text{ in } \mathcal{D}. \tag{5.6}$$

The overline notation indicates a quantity averaged over the microscale. Formally, one can extend the quantities defined in the pore space P by 0 inside the perforations G, allowing for an average over the entire cell Y. For a scalar variable $v(t,\mathbf{x},\mathbf{y})$, we define $\overline{v}(t,\mathbf{x}) = \frac{1}{|Y|}\int_Y v(t,\mathbf{x},\mathbf{y})d\mathbf{y} = \int_P v(t,\mathbf{x},\mathbf{y})d\mathbf{y}$. Note that $|Y|$, the volume of Y, is 1. In this way, the average of the highest order term of the phase field, $\overline{\phi_0}(t,\mathbf{x})$, will correspond to the porosity at time t at the macroscale location $\mathbf{x}$.

5.3.3. Momentum conservation equation. The dominating $O(\varepsilon^{-1})$ term in (5.1c) yields

$$\phi_0^\delta \nabla_{\mathbf{y}} p_0 = \mathbf{0},$$

meaning that $p_0 = p_0(t,\mathbf{x})$ is independent of $\mathbf{y}$. The $O(1)$ terms give

$$\phi_0^\delta(\nabla_{\mathbf{x}} p_0 + \nabla_{\mathbf{y}} p_1) = \mu_f \phi_0^\delta \nabla_{\mathbf{y}}^2\left(\phi_0^\delta \mathbf{q}_0\right) - \frac{K}{\lambda}\frac{(1-\phi_0)n}{\phi_0+n}\mathbf{q}_0. \tag{5.7}$$

We use the linearity of the equation and determine p_1 and $\mathbf{q}_0$ in terms of (the gradient of) p_0. With $\Pi^j(t,\mathbf{x},\mathbf{y})$ and $\mathbf{w}^j(t,\mathbf{x},\mathbf{y})$ solving the cell problems

$$\begin{aligned} \phi_0^\delta(\mathbf{e}_j + \nabla_{\mathbf{y}}\Pi^j) + \mu_f\phi_0^\delta\nabla_{\mathbf{y}}^2\left(\phi_0^\delta\mathbf{w}^j\right) &= \frac{K}{\lambda}\frac{(1-\phi_0)n}{\phi_0+n}\mathbf{w}^j && \text{in } P,\\ \nabla_{\mathbf{y}} \cdot \left(\phi_0^\delta \mathbf{w}^j\right) &= 0 && \text{in } P,\\ \mathbf{w}^j &= \mathbf{0} && \text{on } \Gamma_P,\\ \text{periodicity in } \mathbf{y} \text{ across } \partial Y, & && j \in \{1,\dots,\dim\}, \end{aligned} \tag{5.8}$$

we observe that

$$p_1(t,\mathbf{x},\mathbf{y}) = \sum_{j=1}^{\dim} \Pi^j(t,\mathbf{x},\mathbf{y})\partial_{x_j} p_0(t,\mathbf{x}),$$
$$\mathbf{q}_0(t,\mathbf{x},\mathbf{y}) = -\sum_{j=1}^{\dim} \mathbf{w}^j(t,\mathbf{x},\mathbf{y})\partial_{x_j} p_0(t,\mathbf{x})$$

now fulfill (5.5) and (5.7). The boundary condition for $\mathbf{w}^j$ on Γ_P follows from $\mathbf{q}_0 = \mathbf{0}$ on Γ_P. Note that the cell problems are solved in $\mathbf{y}$ for a fixed $\mathbf{x}$. Hence, as with the phase field cell problem, one can solve for single pores independently.

Multiplying by ϕ_0^δ in the last equality and averaging over Y gives

$$\overline{\phi_0^\delta \mathbf{q}_0} = -\mathcal{K}\nabla_{\mathbf{x}} p_0 \quad \text{in } \mathcal{D}, \tag{5.9}$$

where the components of the *permeability tensor* $\mathcal{K}(t,\mathbf{x})$ are given by

$$k_{ij}(t,\mathbf{x}) = \int_P \phi_0^\delta w_i^j \, d\mathbf{y} \quad \text{with } i,j \in \{1,\dots,\dim\}.$$

Here, w_i^j are the components of $\mathbf{w}^j$, which are the solutions of the cell problems (5.8) with the continuous extension $\mathbf{w}^j = \mathbf{0}$ inside the grain.

5.3.4. Ion conservation equation. The dominating $O(\varepsilon^{-2})$ term from the ion conservation equation (5.1d) and dominating $O(\varepsilon^{-1})$ term from the corresponding boundary condition (5.1f) give

$$\begin{aligned} \nabla_{\mathbf{y}} \cdot \left(\phi_0^\delta \nabla_{\mathbf{y}} u_0\right) &= 0 && \text{in } P, \\ \phi_0^\delta \nabla_{\mathbf{y}} u_0 \cdot \mathbf{n}_P &= 0 && \text{on } \Gamma_P, \end{aligned}$$

along with periodicity in $\mathbf{y}$. This implies that $u_0 = u_0(t,\mathbf{x})$ is independent of $\mathbf{y}$.

Further, the $O(\varepsilon^{-1})$ terms from (5.1d) and $O(1)$ terms from (5.1f) give

$$\begin{aligned} \nabla_{\mathbf{y}} \cdot \left(\phi_0^\delta(\nabla_{\mathbf{x}} u_0 + \nabla_{\mathbf{y}} u_1)\right) &= 0 && \text{in } P, \\ \phi_0^\delta(\nabla_{\mathbf{x}} u_0 + \nabla_{\mathbf{y}} u_1) \cdot \mathbf{n}_P &= 0 && \text{on } \Gamma_P, \end{aligned}$$

where we used (5.5) for the convective term. We exploit again the linearity of the problem and formulate $u_1(t,\mathbf{x},\mathbf{y})$ in terms of (the derivatives of) $u_0(t,\mathbf{x})$. We let the weight functions $\omega^j(t,\mathbf{x},\mathbf{y})$ solve the cell problems

$$\begin{aligned} \nabla_{\mathbf{y}} \cdot \left(\phi_0^\delta(\nabla_{\mathbf{y}} \omega^j + \mathbf{e}_j)\right) &= 0 && \text{in } P, \\ \phi_0^\delta(\nabla_{\mathbf{y}} \omega^j + \mathbf{e}_j) \cdot \mathbf{n}_P &= 0 && \text{on } \Gamma_P, \\ \text{periodicity in } \mathbf{y} \text{ across } \partial Y, \qquad & && j \in \{1,\dots,\dim\}, \end{aligned} \tag{5.10}$$

As earlier, the cell problems are solved in $\mathbf{y}$ for a fixed $\mathbf{x}$. Then, for an arbitrary $\tilde{u}_1 = \tilde{u}_1(t,\mathbf{x})$, we obtain that

$$u_1(t,\mathbf{x},\mathbf{y}) = \tilde{u}_1(t,\mathbf{x}) + \sum_{j=1}^{\dim} \omega^j(t,\mathbf{x},\mathbf{y})\partial_{x_j} u_0(t,\mathbf{x}).$$

As will follow from below, only $\nabla_{\mathbf{y}} u_1$ will be needed for obtaining the upscaled model; therefore the function $\tilde{u}_1$ plays no role in the upscaling, and it is not necessary to specify it.

The $O(1)$ terms from (5.1d) and $O(\varepsilon)$ terms from (5.1f) give

$$\begin{aligned} \partial_t\big(\phi_0^\delta(u_0-u^*)\big)+\nabla_{\mathbf{x}}\cdot\big(\phi_0^\delta \mathbf{q}_0 u_0\big)+\nabla_{\mathbf{y}}\cdot\mathbf{A} & \\ = D\big(\nabla_{\mathbf{y}}\cdot\mathbf{B}+\nabla_{\mathbf{x}}\cdot\big(\phi_0^\delta(\nabla_{\mathbf{x}}u_0+\nabla_{\mathbf{y}}u_1)\big)\qquad & \text{in } \mathcal{D}\times P,\\ \mathbf{B}\cdot\mathbf{n}_P=0 & \text{on } \Gamma_P. \end{aligned}$$

where $\mathbf{A}=\phi_1\mathbf{q}_0u_0+\phi_0^\delta\mathbf{q}_1u_0+\phi_0^\delta\mathbf{q}_0u_1$ and $\mathbf{B}=\phi_0^\delta\nabla_{\mathbf{x}}u_1+\phi_0^\delta\nabla_{\mathbf{y}}u_2+\phi_1\nabla_{\mathbf{x}}u_0+\phi_1\nabla_{\mathbf{y}}u_1$. The above equation contains derivates in both $\mathbf{x}$ and $\mathbf{y}$. To find the upscaled model, we integrate in $\mathbf{y}$ over the domain P, apply Gauss's theorem in $\mathbf{y}$, and use the boundary condition on Γ_P and the periodicity requirement to remove the $\nabla_{\mathbf{y}}\cdot\mathbf{A}$ and $\nabla_{\mathbf{y}}\cdot\mathbf{B}$ terms. For the velocity terms in $\mathbf{A}$, we also apply the boundary condition (5.1g), which gives $\mathbf{q}_0=\mathbf{q}_1=\mathbf{0}$ on Γ_P. This leads to the upscaled reaction-advection-diffusion equation

$$\partial_t\big(\overline{\phi_0^\delta}(u_0-u^*)\big)+\nabla_{\mathbf{x}}\cdot\big(\overline{\phi_0^\delta\mathbf{q}_0}u_0\big)=D\nabla_{\mathbf{x}}\cdot(\mathcal{A}\nabla_{\mathbf{x}}u_0)\text{ in }\mathcal{D}. \tag{5.11}$$

The components of the matrix $\mathcal{A}(t,\mathbf{x})$ are

$$a_{ij}(t,\mathbf{x})=\int_P \phi_0^\delta(\delta_{ij}+\partial_{y_i}\omega^j)d\mathbf{y}\quad \text{with } i,j\in\{1,\dots,\dim\},$$

where ω^j is the solution of the cell problem (5.10). Hence, the upscaled ion conservation equation (5.11) is to be solved for $\mathbf{x}\in\mathcal{D}$ only but receives information from the microscale $\mathbf{y}$ through the effective diffusion matrix and the effective velocity.

5.4. Summary of upscaled equations. To summarize, the upscaled system of equations consists of the three equations (5.6), (5.9), and (5.11) on the macroscale for the unknowns $\overline{\phi\mathbf{q}_0}(t,\mathbf{x})$, $p_0(t,\mathbf{x})$ and $u_0(t,\mathbf{x})$. The upscaled system is completed by three supplementary cell problems (5.4), (5.8), and (5.10) to be solved locally in each single pore, providing effective properties for the upscaled system.

The regularization δ was kept throughout the upscaling procedure for consistency. We introduced this regularization for avoiding a degeneracy in the system, which would create difficulties in the numerical implementations. For the upscaled model, these difficulties are encountered in the cell problems. Hence, we only consider ϕ_0^δ in the effective properties and set $\delta=0$ in (5.6), (5.9), and (5.11). Then, for macroscale $\mathbf{x}\in\mathcal{D}$ and for $t>0$,

$$\begin{aligned} \nabla_{\mathbf{x}}\cdot(\overline{\phi_0\mathbf{q}_0})=0 & \quad \text{in } \mathcal{D},\\ \overline{\phi_0\mathbf{q}_0}=-\mathcal{K}\nabla_{\mathbf{x}}p_0 & \quad \text{in } \mathcal{D},\\ \partial_t\big(\overline{\phi_0}(u_0-u^*)\big)+\nabla_{\mathbf{x}}\cdot(\overline{\phi_0\mathbf{q}_0}u_0)=D\nabla_{\mathbf{x}}\cdot(\mathcal{A}\nabla_{\mathbf{x}}u_0) & \quad \text{in } \mathcal{D}, \end{aligned}$$

where the phase field $\phi_0(t,\mathbf{x},\mathbf{y})$ is updated locally in each pore by solving

$$\begin{aligned} \lambda^2\partial_t\phi_0+\gamma P'(\phi_0)=\gamma\lambda^2\nabla_{\mathbf{y}}^2\phi_0-4\lambda\phi_0(1-\phi_0)\frac{1}{u^*}f(u_0)\qquad & \text{in } P,\\ \nabla_{\mathbf{y}}\phi_0\cdot\mathbf{n}_P=0 & \text{on } \Gamma_P \end{aligned}$$

for all $\mathbf{x} \in \mathcal{D}$ and $t > 0$. The effective matrices $\mathcal{K}(t, \mathbf{x})$ and $\mathcal{A}(t, \mathbf{x})$ are found through

$$
\begin{aligned}
k_{ij}(t, \mathbf{x}) &= \int_P \phi_0^\delta w_i^j d\mathbf{y}, \text{ where} \\
\phi_0^\delta(\mathbf{e}_j + \nabla_{\mathbf{y}} \Pi^j) + \mu_f \phi_0^\delta \nabla_{\mathbf{y}}^2 \left(\phi_0^\delta \mathbf{w}^j\right) &= \frac{K}{\lambda} \frac{(1-\phi_0)n}{\phi_0 + n} \mathbf{w}^j && \text{in } P, \\
\nabla_{\mathbf{y}} \cdot \left(\phi_0^\delta \mathbf{w}^j\right) &= 0 && \text{in } P, \\
\mathbf{w}^j &= \mathbf{0} && \text{on } \Gamma_P,
\end{aligned}
$$

and

$$
\begin{aligned}
a_{ij}(t, \mathbf{x}) &= \int_P \phi_0^\delta (\delta_{ij} + \partial_{y_i} \omega^j) d\mathbf{y}, \text{ where} \\
\nabla_{\mathbf{y}} \cdot \left(\phi_0^\delta (\nabla_{\mathbf{y}} \omega^j + \mathbf{e}_j)\right) &= 0 && \text{in } P, \\
\phi_0^\delta (\nabla_{\mathbf{y}} \omega^j + \mathbf{e}_j) \cdot \mathbf{n}_P &= 0 && \text{on } \Gamma_P
\end{aligned}
$$

for $i, j \in \{1, \ldots, \dim\}$. The unknowns $\mathbf{w}^j(t, \mathbf{x}, \mathbf{y})$, $\Pi^j(t, \mathbf{x}, \mathbf{y})$, and $\omega^j(t, \mathbf{x}, \mathbf{y})$ fulfill periodicity requirements in $\mathbf{y}$ across ∂Y.

6. Numerical experiments for the upscaled model. To illustrate the behavior of the phase field model and its dependence on the diffuse interface width and on the upscaling parameter, we consider two examples. First, we will solve the cell problems for various choices of λ and compare our solution to the corresponding sharp-interface solution, showing how the effective ion diffusivity and the flow permeability depend on the width of the diffuse interface. Second, to illustrate the behavior of the full system of equations, while at the same time addressing the effect of the upscaling, we consider a thin strip. The thin strip allows for an upscaled model where the effective quantities are known explicitly, allowing us to easily address the influence of ε. Note that in all examples, we solve using the corresponding nondimensional model and that all specified parameters are also nondimensional.

6.1. Solutions to cell problems. For sharp-interface models, cell problems for flow and diffusion for moving-boundary problems using a level-set formulation have been derived in [11, 47]. Note that in both formulations, the local reaction rate is uniform inside each pore as the local ion concentration is constant (cf. subsection 5.3.4). Hence, if the minerals are initially shaped as circles (or cylinders), the mineral layer will evolve in a radially symmetric manner, and the mineral remains a circle (or cylinder); see [47]. Hence, the level-set formulation can be rewritten into an equation for the radius $R(t, \mathbf{x})$ of the solid (grain and mineral), where the cell problems depend on $R(t, \mathbf{x})$ [13, 47]. In the radially symmetric case, the effective ion diffusivity and the permeability will be scalar quantities.

We adopt a similar approach here by solving the cell problems (5.8) and (5.10) to determine the effective permeability and ion diffusivity by assuming that the phase field has a smooth transition (of $O(\lambda)$) at some distance R from the center of the cell. We do not attempt to determine permeability and diffusivity curves as functions of R as in [13, 47] (see, e.g., Figure 3 in [47]), but instead we choose some values of R and investigate the behavior as we let the diffuse interface width λ vary.

The cell problems (5.8) and (5.10) are discretized using a control volume method on a staggered cartesian grid as in section 4, where the cell problem unknowns ω^j

and Π^j are defined in the centers of the control volumes, and the vectors $\mathbf{w}^j$ are at the edges. The grid is uniform and quadratical with 800 grid cells in each direction, so that we have at least eight grid cells through the diffuse transition zone for the smallest λ. Note that the size of the nonreactive part G does not affect the resulting values of the effective variables as long G is well within the mineral phase. For all cell problems, we use a regularization of $\delta = 10^{-8}$.

Remark 6.1. Specifying a phase field corresponding to a circular mineral with radius R is not straightforward as no analytical expression exists. An approximate phase field can be found by assuming radial symmetry and considering the reaction-free version of (5.4) in polar coordinates. That is, we seek $\phi(t, r)$ solving

$$\lambda^2 \partial_t \phi + \gamma P'(\phi) = \gamma \lambda^2 \frac{1}{r} \partial_r (r \partial_r \phi). \tag{6.1}$$

Because of the nonconservative property of the Allen–Cahn equation, a radially symmetric phase field drop will always shrink towards the center due to curvature effects. Using this, we consider the initial condition

$$\phi(t = 0, r) = \frac{1}{1 + \exp(-4(r - R_0)/\lambda)}, \tag{6.2}$$

where R_0 is larger than the radius R, which is the mineral radius for which we seek a phase field. Following from the curvature-driven movement, the mineral will shrink according to the radial Allen–Cahn equation (6.1). The simulation is stopped when the radius of the transition region reaches R, that is, when $\phi = 0.5$ at $r = R$. Hence, this resulting phase field is used when solving the cell problems. As boundary conditions, we apply $\phi = 0$ at $r = 0$ and $\phi = 1$ at $r = 1$. It could be tempting to directly specify (6.2) with $R_0 = R$ as the phase field, but this would not fulfill the steady-state version of (6.1). Although (6.2) has a structure similar to (3.7), which is the solution of the one-dimensional steady-state version of the Allen–Cahn equation, this finding cannot be extended to the radially symmetric case due to the structure of the Laplace operator in polar coordinates. This also means that the initial condition (6.2) is only an approximate initial condition.

6.1.1. Permeability. For the cell problem (5.8) providing the permeability, we consider mineral radii of $R = 0.2,\ 0.3,\ 0.4$. The corresponding permeability values for these mineral radii are $\mathcal{K} = 3.3 \times 10^{-2},\ 1.1 \times 10^{-2},\ 1.8 \times 10^{-3}$, respectively [13]. The applied values of λ in (6.2) will be $\lambda = 0.05,\ 0.04,\ 0.03,\ 0.02,\ 0.01,\ 0.0075,\ 0.005$. In Figure 6, the phase field permeability values are compared to the permeability values resulting from the corresponding sharp-interface models. It becomes clear that the phase field permeability values are approaching those for the sharp-interface models as the values of λ are decreasing. However, the relative errors are large and for $\lambda = 0.01$ are equal to 5%, 7%, and 15% for $R = 0.2,\ 0.3,\ 0.4$, respectively. These deviations can be explained by the fact that flow takes place in the diffuse transition zone, which enhances the flow through the entire cell and hence overestimates the permeability. This effect is diminished when the parameter K in the phase field cell problem (5.8) is increased, but larger values of K could also lead to an underestimation of the permeability if λ is large. For the results in Figure 6, $K = 25$ was used. Hence, finding a good choice for the interpolation function $g(\phi, \lambda)$ in (2.5c) is essential in the numerical implementation.

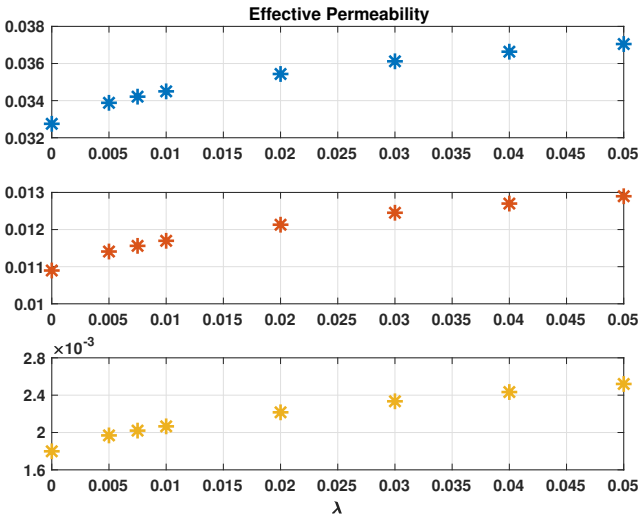

FIG. 6. *Permeability values for $R = 0.2$ (top), $R = 0.3$ (middle), and $R = 0.4$ (bottom) for various values of λ. The sharp-interface values are plotted at $\lambda = 0$.*

6.1.2. Effective ion diffusivity. For the effective diffusivity cell problem (5.10), we consider the same values for R and λ. The effective diffusivities for the sharp-interface model are, for these three values of R, $\mathcal{A} = 0.78,\ 0.56,\ 0.32$, respectively. These values have been found by solving the corresponding sharp-interface cell problems for the diffusion tensor, whose formulation can be found, e.g., in [47], using the PDE toolbox in MATLAB on recursively finer grids until four digits of accuracy are obtained. The phase field effective diffusion values are compared to the corresponding sharp-interface effective diffusion values in Figure 7. Although the phase field values seemingly converge towards a slightly different value than the value provided by the sharp-interface model, it is worth noting that the relative errors are rather small ($< 0.3\%$ in all cases), and hence the effective diffusion tensors are well approximated even for large values of λ. Note that when defining the transition zone as being where $\phi = 0.5$ leads to a slightly overestimated size of the grain as the transition zone spreads out radially, which can explain why the diffusion values approaches a value that is slightly too low. For example, for $R = 0.3$ the relative difference between the true porosity and that found through Remark 6.1 using $\lambda = 0.01$ is 0.03%. Other potential sources of error would be the difference in numerical solvers between the diffuse and sharp-interface discretizations.

6.2. Flow through a thin strip. A simple but instructive test case is when the general model (5.1) is formulated in a two-dimensional thin strip, mimicking the flow through a long pore. In this case, the scale separation is defined through the ratio $\varepsilon = \ell/L$ between the width ℓ and the length L of the strip. In the nondimensional case, the domain of the thin strip is $(x, y) \in (0, 1)^2$ due to different scaling of the transversal coordinate y. Note that y now plays the role of the transversal variable, rather than a local one, but is still scaled as $y = \varepsilon^{-1}x$ and represents the direction where rapid changes are occurring.

The model equations for the original two-dimensional strip are (5.1). The resulting effective model for the thin strip is one-dimensional and is found through

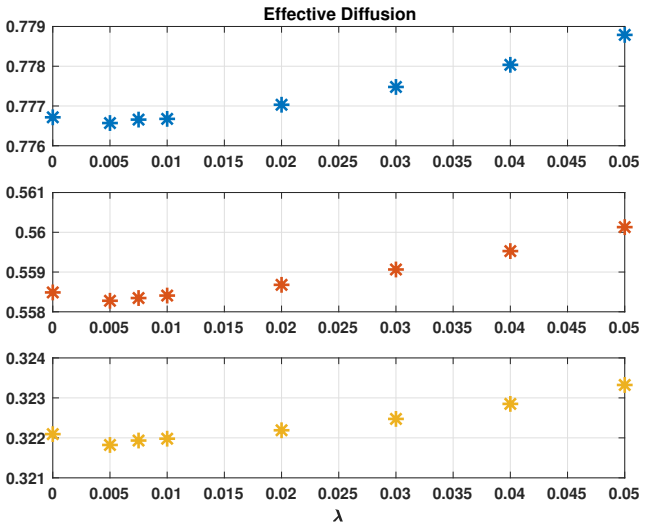

FIG. 7. *Effective diffusion values for $R = 0.2$ (top), $R = 0.3$ (middle), and $R = 0.4$ (bottom) for various values of λ. The sharp-interface values are plotted at $\lambda = 0$.*

asymptotic expansions and transversal averaging of the model equations. Sharp interface formulations for models in a thin strip and that consider reactive transport leading to changes in the pore geometry have been formulated and upscaled in [10, 12, 28, 48].

When transversally averaging the model equations, we use a slight reformulation for the phase field equation. Assuming that the mineral is only present as a layer on the upper and lower walls of the strip, and using symmetry across the middle of the strip, we approximate the phase field for the lower half of the strip by

$$\phi(t,x,y) = \frac{1}{1+e^{-4(y-d)/\lambda}}, \tag{6.3}$$

where $d(t,x)$ is the mineral layer width. This form of the phase field is similar to that used in the matched asymptotic expansions (3.7); however, it remains an approximation because zero Neumann conditions at the bottom wall $y = 0$ and symmetry at $y = 1/2$ are not fulfilled. With the unknowns $d(t,x)$, $\overline{\phi}(t,x)$, $u_0(t,x)$, and $\overline{\phi q_0^x}(t,x)$, the upscaled equations obtained by transversal averaging are

$$\partial_t d = f(u_0), \tag{6.4a}$$

$$\overline{\phi} = 1 + \frac{\lambda}{2}\log\left(1+e^{-4(0.5-d)/\lambda}\right) - \frac{\lambda}{2}\log\left(1+e^{4d/\lambda}\right), \tag{6.4b}$$

$$\overline{\phi q_0^x} = 1, \tag{6.4c}$$

$$\partial_t(\overline{\phi}(u_0-u^*)) = -\partial_x(\overline{\phi q_0^x}(u_0-u^*)) + D\partial_x(\overline{\phi}\partial_x(u_0-u^*)) \tag{6.4d}$$

for $x \in (0,1)$ and $t > 0$. The derivation of these equations can be found in Appendix A. Note the absence of a momentum conservation equation; hence the pressure is not obtained here. Further, we assume that clogging of the pore due to mineral precipitation does not occur, which means that no degeneracy occurs. This allows taking $\delta = 0$, but performing the upscaling for $\delta > 0$ is straightforward.

The original equations (5.1) are formulated on the scaled strip $(x,y) \in [0,1]^2$ but using symmetry at $y = 0.5$. Therefore, only half of the strip needs to be considered.

For both the original system (5.1) and the transversally averaged system (6.4), we design an example including dissolution. We let $u_0(t=0) = u^\varepsilon(t=0) = 0.5$ in the entire domain initially and inject an ion concentration of $u_0 = u^\varepsilon = 0.25$ at $x = 0$. At the outlet $x = 1$ we assume zero Neumann condition for the ion concentration. The reaction rate is chosen to be $f(u) = u^2/0.5^2 - 1$, corresponding to an equilibrium concentration of $u_{\text{eq}} = 0.5$. Hence, net dissolution will occur when injecting a lower ion concentration. Initially, the strip is assumed to be halfway filled with a mineral layer at the top and the bottom, that is, $d(t=0) = 0.25$. The phase field in the original equations is initialized with (6.3) using $d = 0.25$. Also, we apply a zero Neumann condition for the phase field at both the inlet and the outlet. The original model (5.1) is initiated with constant pressure and zero velocity. In the upscaled system (6.4), the inlet condition $\overline{\phi q_0^x} = 1$ also gives the flow through the strip. For the original equations (5.1), the inlet condition for the horizontal component of the flow rate $\mathbf{q}^\varepsilon$, $q^{\varepsilon,x}$, is formulated using a time-dependent parabolic profile such that $q_x^\varepsilon = 0$ at $y = d(t,0)$, $\partial_y q^{\varepsilon,x} = 0$ at the symmetry line $y = 0.5$, and $\overline{\phi^\varepsilon q^{\varepsilon,x}} = 1$ is fulfilled. The outlet condition for pressure is a zero Neumann condition.

The following (nondimensional) constants have been used in the simulations:

$$D = 1, \quad u^* = 1, \quad \gamma = 0.0075, \quad K = 25, \quad \rho_f = 1, \quad \mu_f = 1.$$

The value of γ is chosen small to ensure low surface curvature effects, while the value of K is chosen large to avoid too much flow in the diffuse transition zone. Also note that the mineral concentration is chosen artificially low so that large changes in the mineral width occur [48]. We let $\delta = 10^{-6}$ in the original model (5.1) for all simulations.

Similarly as in subsection 6.1 and section 4, both the original equations (5.1) and the averaged system (6.4) are discretized using a control volume method on a staggered cartesian grid where ion concentration, pressure, and phase field are defined in the centers of the control volumes, and the velocities are defined in the centers of the edges. For the original equations, rectangular grids are used, where the resolution in the transversal direction is fine enough to resolve the diffuse transition zone properly.

6.2.1. Comparison to sharp-interface formulation. For the upscaled system of equations (6.4), we can compare the obtained solution to similar upscaled models based on a sharp-interface formulation, such as those found in [10, 48]. Discretizing the sharp-interface model with the same method, and choosing the same initial and boundary conditions, we can investigate the effect of the diffuse interface λ on the model variables.

The are some minor differences in ion concentration u_0 and, accordingly, in the value of mineral width d as the reaction rate depends on u_0. Figure 8 shows the ion concentrations in the sharp-interface model and in the phase field model for various values of λ at $t = 0.5$. For smaller values of λ, the ion concentration approaches the values found through the sharp-interface model. The differences in values for the mineral width are small (the largest absolute difference for $\lambda = 0.05$ is 0.003).

6.2.2. Comparison to original two-dimensional formulation. We can also check the quality of the upscaling procedure, namely whether the transversal averages of the output from the original equations (5.1) approach the model output found by the upscaled model (6.4) as ε approaches zero. For this comparison we fix a value of λ and let ε vary. For simplicity we consider $\lambda = 0.05,\ 0.01$, and $\varepsilon = 0.1,\ 0.05,\ 0.025,\ 0.01,\ 0.005$, where $\varepsilon = 0.005$ corresponds to a strip that is 200

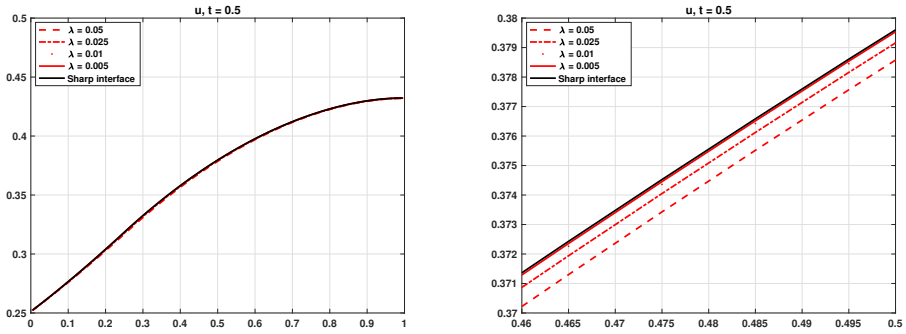

FIG. 8. *Ion concentration inside thin strip at* $t = 0.5$. *Right figure shows zoomed-in view near the middle of the strip, where the largest differences between the model runs are found.*

times longer than its width. A typical snapshot from a simulation, with $\lambda = 0.05$ and $\varepsilon = 0.1$, is shown in Figure 9. Even for such a "large" value of ε, the derivatives with respect to y of, e.g., ion concentration, is practically zero. The flow field is found through solving Navier–Stokes equations, and the along-strip component shows a parabola-like profile as expected for this regime. Some flow inside the diffuse interface can be seen.

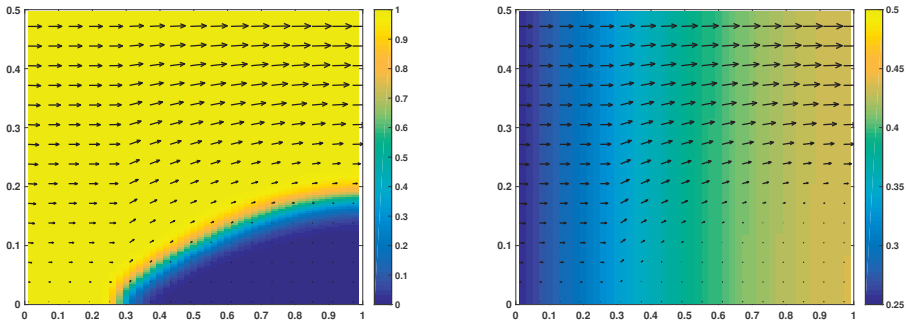

FIG. 9. *Phase field (left) and ion concentration (right) in a thin strip at* $t = 0.5$. *Note that the y-axis is scaled to fit between* 0 *and* 0.5 *but should be between* 0 *and* 0.5ε. *Velocity field is given as vector overlay and is mainly along the strip. The transversal component of the velocity field has been scaled with* $1/\varepsilon$. *For this simulation,* $\varepsilon = 0.1$ *and* $\lambda = 0.05$. *The domain was discretized with* 50 *control volumes in the x-direction and* 150 *control volumes in the y-direction.*

By vertically averaging the results from the original equations (5.1) and comparing them to the results from the already upscaled model (6.4), we find in general good correspondence. There is little variability in the transversal direction for ion concentration already for relatively large values of ε, as illustrated in Figure 9 for $\varepsilon = 0.1$. Hence, the averaged ion concentration does not deviate much when decreasing ε. However, some differences are found in the dissolution of the mineral between the two-dimensional model (5.1) and the upscaled model (6.4). These differences do not change with smaller ε. The upscaled system of equations uses directly $\partial_t d = f(u)/u^*$, which is equivalent to the reaction rate found in a sharp-interface model, while the original phase field equation still experiences an effect from the interface width λ in

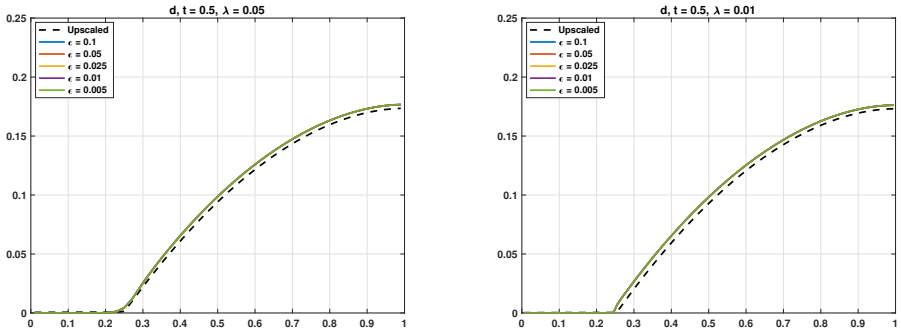

FIG. 10. *Width of mineral layer $d(t,x)$ inside (the lower half of) the thin strip at $t = 0.5$ for $\lambda = 0.05$ (left) and $\lambda = 0.01$ (right). Note that the colored lines, corresponding to averaged results from the original equations* (5.1)*, are (almost) on top of each other. The mineral width is found through the phase field by $(0.5 - 0.5\overline{\phi}^{\varepsilon})$. (See online version for color.)*

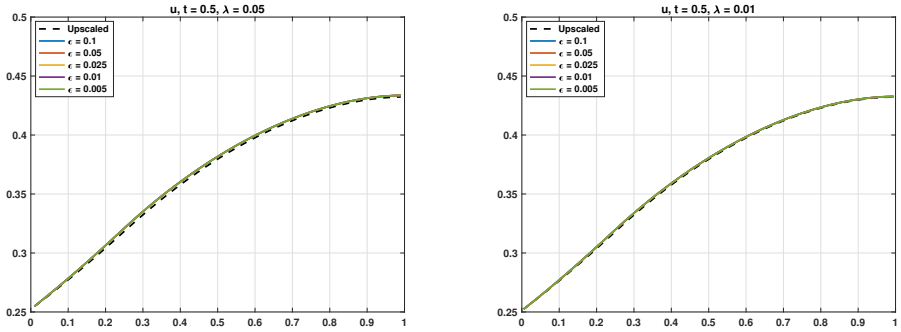

FIG. 11. *Transversally averaged ion concentration inside a thin strip at $t = 0.5$ for $\lambda = 0.05$ (left) and $\lambda = 0.01$ (right). Note that the colored lines, corresponding to averaged results from the original equations* (5.1)*, are (almost) on top of each other. (See online version for color.)*

the reaction rate. Also, the upscaled model uses an approximated phase field which does not fulfill the boundary conditions at the top and bottom boundaries. However, as seen from Figures 10 and 11, the differences in d and u are very small already for $\lambda = 0.05$.

7. Conclusions. We have derived a phase field model for reactive transport with mineral precipitation and dissolution. Compared to other modeling approaches involving free boundaries moving due to precipitation and dissolution, the phase field model has the advantage of being formulated in a fixed domain. The free boundary is then replaced by a diffuse interface region.

The model proposed here extends the one in [38] by incorporating fluid flow. The extension provides mass and momentum conservation by modifying the Navier–Stokes equations, where the phase field variable is incorporated. The momentum conservation equation is further modified by adding a source term to ensure no flow in the pure mineral phase. Using matched asymptotic expansions, we have shown that the phase field model reduces to the expected sharp-interface model when the width of the diffuse interface approaches zero. Hence, the phase field model captures fluid

flow and solute transport in the fluid phase and, as anticipated, no-slip and Rankine–Hugoniot jump conditions at the evolving fluid-mineral interface. The behavior of the phase field model has been illustrated by considering two numerical experiments where a mineral dissolves when located in flow fields of various strengths. Comparing to a benchmark [33], we find the phase field model to behave qualitatively and quantitatively as expected, although with a slight overestimation of the dissolution rate.

When considering a porous medium, the model proposed here can be seen as a pore scale model. By considering the medium as periodically perforated, an upscaled counterpart of the phase field model is obtained by means of homogenization techniques. The resulting effective equations are valid at the Darcy scale. We obtain the cell problems that provide the effective ion diffusion as in [38]. Here we also obtain cell problems for obtaining the effective permeability and porosity. In particular, since the porosity in a cell is the average of the phase field over that cell, the model also provides an equation describing the evolution of the porosity in time, depending on the macroscale location. Numerical experiments show the behavior of the cell problems with respect to the width of the diffuse interface, where the diffusive cell problems provide accurate results for relatively large values of the width of the diffuse interface, while the permeability is prone to being overestimated.

The use of a phase field model instead of a sharp-interface formulation avoids some potential numerical pitfalls, as there is no need to, e.g., solve the level-set equation. Using a diffuse interface as a replacement for a sharp-interface simplifies the development of numerical simulation tools but also introduces a relaxation which can lead to inaccurate numerical results. As seen from the numerical experiments, the mineral dissolved a bit faster than expected due to the nonconservative property of the Allen–Cahn equation, and the permeability could easily be overestimated or underestimated due to artificial flow in the diffuse transition zone. Hence, using small values for the interface diffusivity and of diffuse interface width are important for obtaining a good representation of the flow at the pore scale or in the cell problems, which in turn puts constraints on how fine the grid has to be near the diffuse interface.

Appendix A. Thin strip model. Here we derive the averaged thin strip model using a phase field formulation, as given in (6.4). The starting point is the original phase field model for a porous medium (5.1), but formulated in a thin strip having width ℓ and length L, such that $\varepsilon = \ell/L$ defines the scale separation. Hence, in the nondimensional setting, the strip has width and length 1 but where derivatives in the y-direction (across the strip) are scaled with $1/\varepsilon$. Hence, for a dummy variable $v(x, y)$ one gets

$$\nabla v(x, y) = \partial_x v \mathbf{i} + \frac{1}{\varepsilon} \partial_y v \mathbf{j},$$

where $\mathbf{i}$ and $\mathbf{j}$ are unit vectors in the along-strip and transversal direction. Due to symmetry we consider only the lower half of the strip. As explained earlier, the phase field approaching value 1 in the fluid part and 0 in the mineral part is given by

$$\phi(t, x, y) = \frac{1}{1 + e^{-4(y-d)/\lambda}}, \tag{A.1}$$

where $y = d(t, x)$ defines the transition between fluid and mineral where $\phi = 0.5$. This formulation uses $d(t, x)$ as an unknown as in sharp-interface models but still incorporates a phase field variable that affects the model formulation. However, as ϕ in (A.1) does not fulfill the zero Neumann and symmetry boundary conditions, we are

making a small error by using this phase field. Here we derive the upscaled (transversally averaged) model for the current formulation. As there will be no problems with degeneracy in the equations for the resulting thin strip model, we let $\delta = 0$. It is, of course, possible to do the transversal averaging also with $\delta > 0$, and would only require the phase field ϕ being replaced with $\phi + \delta$ in the ion and mass conservation equations.

A.1. Equation for $d(t, x)$. The equation for $d(t, x)$ is obtained by inserting (A.1) into the phase field equation (5.1a) and collecting the lowest order terms in ε, $O(\varepsilon^0)$. This gives

$$\lambda^2 \partial_t \phi_0 + \gamma P'(\phi_0) = \gamma \lambda^2 \partial_y^2 \phi_0 - 4\lambda \phi_0 (1 - \phi_0) \frac{1}{u^*} f(u_0).$$

Inserting (A.1) for ϕ, using the equalities

$$\partial_t \phi = -\frac{4}{\lambda} \phi (1 - \phi) \partial_t d,$$

$$\partial_y^2 \phi = \frac{4^2}{\lambda^2} \phi (1 - \phi)(1 - 2\phi),$$

and cancelling equal terms and common factors results in

$$\partial_t d = \frac{1}{u^*} f(u). \tag{A.2}$$

Hence, the phase field $\phi(t, x, y)$ is given by (A.1), where the mineral width $d(t, x)$ follows from (A.2).

Note that the resulting equation for $d(t, x)$ is the same model equation as used in the sharp-interface thin strip formulations of [10, 48]. However, the phase field $\phi(t, x, y)$ will still appear in the upscaled solute transport and flow equations. This allows us to illustrate the behavior of the phase field model with respect to λ and ε in a simple setting.

A.2. Equation for the averaged phase field. The transversally averaged phase field will be needed in the upscaled thin strip model. In view of the symmetry, the transversal average of (A.1) is

$$\overline{\phi} = 2 \int_0^{1/2} \frac{1}{1 + e^{-4(y-d)/\lambda}} dy = 1 + \frac{\lambda}{2} \log\left(1 + e^{-\frac{4}{\lambda}(0.5-d)}\right) - \frac{\lambda}{2} \log\left(1 + e^{\frac{4}{\lambda} d}\right).$$

A.3. Equation for mass conservation. The lowest order term arising from the mass conservation equation (5.1b) yields

$$\partial_y (\phi q_0^y) = 0,$$

which, together with the boundary condition (5.1g), gives that the lowest order transversal velocity component q_0^y is independent of y. The next order provides

$$\partial_x (\phi q_0^x) + \partial_y (\phi q_1^y) = 0,$$

where q_0^x is the lowest order along-strip velocity component, and q_1^y is the first-order transversal velocity component. This equation is integrated in y from 0 to $1/2$, which, together with boundary condition (5.1g) at $y = 0$ and symmetry at $y = 1/2$, gives

$$\partial_x (\overline{\phi q_0^x}) = 0.$$

A.4. Equation for average flow rate. Inserting asymptotic expansions into (5.1c), from the lowest order term, one gets

$$\phi \partial_y p_0 = 0,$$

implying that $p_0 = p_0(t, x)$ is independent of y. The horizontal (along the strip) component of the $O(1)$ terms provides

$$0 = -\phi \partial_x p_0 + \mu_f \phi \partial_y^2 (\phi q_0^x) - \frac{K}{\lambda} \frac{(1-\phi)n}{\phi + n} q_0^x.$$

We let $v = \phi q_0^x$ represent the unknown and insert the expression for ϕ, (A.1), when necessary. Then,

$$\mu_f v'' - \frac{K}{\lambda} \frac{n e^{-4(y-d)/\lambda} (1 + e^{-4(y-d)/\lambda})^2}{1 + n(1 + e^{-4(y-d)/\lambda})} v = \partial_x p_0, \tag{A.3}$$

where $'$ indicates derivative with respect to y. The variables t and x appearing in d and p are considered parameters. Hence, we have an inhomogeneous, second-order, linear ODE with nonconstant coefficients. Finding simple analytical expressions for the solution of v is not straightforward. Instead, the boundary condition $\overline{\phi q_0^x} = 1$ can be used to resolve the flow through the strip together with mass conservation. This means that we will not be able to solve the pressure inside the thin strip.

A.5. Equation for ion concentration. Inserting (A.1) for ϕ and asymptotic expansion for u^ε into (5.1d) and equating the lowest order terms yields

$$\partial_y(\phi \partial_y u_0) = 0.$$

Together with the lowest order boundary condition $\phi \partial_y u_0 = 0$ at $y = 0, 1$ and the fact that $\phi > 0$, it follows that

$$u_0 = u_0(t, x).$$

Hence, u_0 is independent of the transversal variable y. Integrating (5.1d) in y from 0 to 1/2, and applying boundary conditions (5.1f) and (5.1g) on the lower boundary and symmetry conditions on $y = 1/2$, results in

$$\int_0^{1/2} \partial_t(\phi(u^\varepsilon - u^*))dy + \int_0^{1/2} \partial_x(\phi q^{\varepsilon,x}(u^\varepsilon - u^*))dy = D \int_0^{1/2} \partial_x(\phi \partial_x(u^\varepsilon - u^*))dy,$$

where $q^{\varepsilon,x}$ is the along-strip component of the $\mathbf{q}^\varepsilon$. Using the asymptotic expansions and the fact that u_0 is independent of y leads to

$$\partial_t(\overline{\phi}(u_0 - u^*)) + \partial_x(\overline{\phi q_0^x}(u_0 - u^*)) = D \partial_x(\overline{\phi} \partial_x(u_0 - u^*)).$$

Acknowledgments. We would like to thank Profs. Christian Rohde (Stuttgart) and Harald Garcke (Regensburg) for useful discussions on the phase field formulation.

REFERENCES

[1] H. Abels and Y. Liu, *Sharp interface limit for a Stokes/Allen–Cahn system*, Arch. Ration. Mech. Anal., 229 (2018), pp. 417–502, https://doi.org/10.1007/s00205-018-1220-x.

[2] A. W. Adamson and A. P. Gast, *Physical Chemistry of Surfaces*, Interscience Publishers, New York, 1967.

[3] A. Agosti, B. Giovanardi, L. Formaggia, and A. Scotti, *A numerical procedure for geochemical compaction in the presence of discontinuous reactions*, Adv. Water Resour., 94 (2016), pp. 332–344, https://doi.org/10.1016/j.advwatres.2016.06.001.

[4] G. Allaire and H. Hutridurga, *Homogenization of reactive flows in porous media and competition between bulk and surface diffusion*, IMA J. Appl. Math., 77 (2012), pp. 788–815.

[5] S. M. Allen and J. W. Cahn, *A microscopic theory for antiphase boundary motion and its application to antiphase domain coarsening*, Acta Metallurgica, 27 (1979), pp. 1085–1095, https://doi.org/10.1016/0001-6160(79)90196-2.

[6] I. Battiato and D. Tartakovsky, *Applicability regimes for macroscopic models of reactive transport in porous media*, J. Contaminant Hydrology, 120-121 (2011), pp. 18–26, https://doi.org/10.1016/j.jconhyd.2010.05.005.

[7] I. Battiato, D. Tartakovsky, A. Tartakovsky, and T. Scheibe, *On breakdown of macroscopic models of mixing-controlled heterogeneous reactions in porous media*, Adv. Water Resour., 32 (2009), pp. 1664–1673, https://doi.org/10.1016/j.advwatres.2009.08.008.

[8] C. Beckermann, H.-J. Diepers, I. Steinbach, A. Karma, and X. Tong, *Modeling melt convection in phase-field simulations of solidification*, J. Comput. Phys., 154 (1999), pp. 468–496, https://doi.org/10.1006/jcph.1999.6323.

[9] F. Boyer, C. Lapuerta, S. Minjeaud, B. Piar, and M. Quintard, *Cahn–Hilliard/Navier–Stokes model for the simulation of three-phase flows*, Transp. Porous Media, 82 (2010), pp. 463–483, https://doi.org/10.1007/s11242-009-9408-z.

[10] C. Bringedal, I. Berre, I. S. Pop, and F. A. Radu, *A model for non-isothermal flow and mineral precipitation and dissolution in a thin strip*, J. Comput. Appl. Math., 289 (2015), pp. 346–355, https://doi.org/10.1016/j.cam.2014.12.009.

[11] C. Bringedal, I. Berre, I. S. Pop, and F. A. Radu, *Upscaling of non-isothermal reactive porous media flow with changing porosity*, Transp. Porous Media, 114 (2016), pp. 371–393, https://doi.org/10.1007/s11242-015-0530-9.

[12] C. Bringedal, I. Berre, I. S. Pop, and F. A. Radu, *Upscaling of nonisothermal reactive porous media flow under dominant Péclet number: The effect of changing porosity*, Multiscale Model. Simul., 14 (2016), pp. 502–533, https://doi.org/10.1137/15M1022781.

[13] C. Bringedal and K. Kumar, *Effective behavior near clogging in upscaled equations for non-isothermal reactive porous media flow*, Transp. Porous Media, 120 (2017), pp. 553–577, https://doi.org/10.1007/s11242-017-0940-y.

[14] G. Caginalp and P. C. Fife, *Dynamics of layered interfaces arising from phase boundaries*, SIAM J. Appl. Math., 48 (1988), pp. 506–518, https://doi.org/10.1137/0148029.

[15] J. W. Cahn and J. E. Hilliard, *Free energy of a nonuniform system* I*: Interfacial free energy*, J. Chem. Phys., 28 (1958), pp. 258–267, https://doi.org/10.1063/1.1744102.

[16] Z. Chen, S. L. Lyons, and G. Qin, *Derivation of the Forchheimer law via homogenization*, Transp. Porous Media, 44 (2001), pp. 325–335, https://doi.org/10.1023/A:1010749114251.

[17] C. Choquet and A. Mikelić, *Rigorous upscaling of the reactive flow with finite kinetics and under dominant Péclet number*, Contin. Mech. Thermodyn., 21 (2009), pp. 125–140, https://doi.org/10.1007/s00161-009-0099-z.

[18] K. R. Daly and T. Roose, *Homogenization of two fluid flow in porous media*, Proc. Roy. Soc. A Math. Phys. Engrg. Sci., 471 (2015), 20140564, https://doi.org/10.1098/rspa.2014.0564.

[19] Y. Davit, C. G. Bell, H. M. Byrne, L. A. Chapman, L. S. Kimpton, G. E. Lang, K. H. L. Leonard, J. M. Oliver, N. C. Pearson, R. J. Shipley, S. L. Waters, J. P. Whiteley, B. D. Wood, and M. Quintard, *Homogenization via formal multiscale asymptotics and volume averaging: How do the two techniques compare?*, Adv. Water Resour., 62, part B (2013), pp. 178–206, https://doi.org/10.1016/j.advwatres.2013.09.006.

[20] M. Dentz, T. L. Borgne, A. Englert, and B. Bijeljic, *Mixing, spreading and reaction in heterogeneous media: A brief review*, J. Contaminant Hydrology, 120-121 (2011), pp. 1–17, https://doi.org/10.1016/j.jconhyd.2010.05.002.

[21] K. R. Elder, M. Grant, N. Provatas, and J. M. Kosterlitz, *Sharp interface limits of phase-field models*, Phys. Rev. E, 64 (2001), 021604, https://doi.org/10.1103/PhysRevE.64.021604.

[22] H. Garcke, C. Hecht, M. Hinze, and C. Kahle, *Numerical approximation of phase field based shape and topology optimization for fluids*, SIAM J. Sci. Comput., 37 (2015), pp. A1846–A1871, https://doi.org/10.1137/140969269.

[23] U. Hornung, ed., *Homogenization and Porous Media*, Interdiscip. Appl. Math. 6, Springer-Verlag, New York, 1996, https://doi.org/10.1007/978-1-4612-1920-0.

[24] D. Jeong and J. Kim, *Conservative Allen–Cahn-Navier–Stokes system for incompressible two-phase fluid flows*, Comput. & Fluids, 156 (2017), pp. 239–246, https://doi.org/10.1016/j.compfluid.2017.07.009.

[25] P. Knabner, C. J. van Duijn, and S. Hengst, *An analysis of crystal dissolution fronts in flows through porous media part* 1: *Compatible boundary conditions*, Adv. Water Resour., 18 (1995), pp. 171–185, https://doi.org/10.1016/0309-1708(95)00005-4.

[26] K. Kumar, M. Neuss-Radu, and I. S. Pop, *Homogenization of a pore scale model for precipitation and dissolution in porous media*, IMA J. Appl. Math., 81 (2016), pp. 877–897, https://doi.org/10.1093/imamat/hxw039.

[27] K. Kumar, I. S. Pop, and F. A. Radu, *Convergence analysis of mixed numerical schemes for reactive flow in a porous medium*, SIAM J. Numer. Anal., 51 (2013), pp. 2283–2308, https://doi.org/10.1137/120880938.

[28] K. Kumar, T. L. van Noorden, and I. S. Pop, *Effective dispersion equations for reactive flows involving free boundaries at the microscale*, Multiscale Model. Simul., 9 (2011), pp. 29–58, https://doi.org/10.1137/100804553.

[29] T. Le Borgne, D. Bolster, M. Dentz, P. de Anna, and A. Tartakovsky, *Effective pore-scale dispersion upscaling with a correlated continuous time random walk approach*, Water Resour. Res., 47 (2011), W12538, https://doi.org/10.1029/2011WR010457.

[30] X. Li, J. Lowengrub, A. Rätz, and A. Voigt, *Solving PDEs in complex geometries: A diffuse domain approach*, Commun. Math. Sci., 7 (2009), pp. 81–107, https://doi.org/10.4310/cms.2009.v7.n1.a4.

[31] S. Metzger and P. Knabner, *Homogenization of Two-Phase Flow in Porous Media from Pore to Darcy Scale: A Phase-Field Approach*, preprint, https://arxiv.org/abs/2002.02531, 2020.

[32] A. Mikelić, V. Devigne, and C. J. van Duijn, *Rigorous upscaling of the reactive flow through a pore, under dominant Peclet and Damkohler numbers*, SIAM J. Math. Anal., 38 (2006), pp. 1262–1287, https://doi.org/10.1137/050633573.

[33] S. Molins, C. Soulaine, N. I. Prasianakis, A. Abbasi, P. Poncet, A. J. C. Ladd, V. Starchenko, S. Roman, D. Trebotich, H. A. Tchelepi, and C. L. Steefel, *Simulation of mineral dissolution at the pore scale with evolving fluid-solid interfaces: Review of approaches and benchmark problem set*, Comput. Geosci., to appear (published online January 23, 2020), https://doi.org/10.1007/s10596-019-09903-x.

[34] S. Molins, D. Trebotich, G. H. Miller, and C. I. Steefel, *Mineralogical and transport controls on the evolution of porous media texture using direct numerical simulation*, Water Resour. Res., 53 (2017), pp. 3645–3661, https://doi.org/10.1002/2016WR020323.

[35] X. Mu, F. Frank, B. Riviere, F. O. Alpak, and W. G. Chapman, *Mass-conserved density gradient theory model for nucleation process*, Ind. Eng. Chem. Res., 57 (2018), pp. 16476–16485, https://doi.org/10.1021/acs.iecr.8b03389.

[36] M. Quintard and S. Whitaker, *Convection, dispersion, and interfacial transport of contaminants: Homogeneous porous media*, Adv. Water Resour., 17 (1994), pp. 221–239, https://doi.org/10.1016/0309-1708(94)90002-7.

[37] M. Quintard and S. Whitaker, *Dissolution of an immobile phase during flow in porous media*, Ind. Eng. Chem. Res., 38 (1999), pp. 833–844, https://doi.org/10.1021/ie980212t.

[38] M. Redeker, C. Rohde, and I. S. Pop, *Upscaling of a tri-phase phase-field model for precipitation in porous media*, IMA J. Appl. Math., 81 (2016), pp. 898–939, https://doi.org/10.1093/imamat/hxw023.

[39] C. Rohde and L. von Wolff, *A Ternary Cahn-Hilliard Navier-Stokes Model for Two Phase Flow with Precipitation and Dissolution*, preprint, https://arxiv.org/1912.09181, 2019.

[40] F. Schlögl, *Chemical reaction models for non-equilibrium phase transitions*, Z. Phys., 253 (1972), pp. 147–161, https://doi.org/10.1007/BF01379769.

[41] M. Schmuck, M. Pradas, G. A. Pavliotis, and S. Kalliadasis, *Upscaled phase-field models for interfacial dynamics in strongly heterogeneous domains*, Proc. Roy. Soc. A Math. Phys. Eng. Sci., 468 (2012), pp. 3705–3724, https://doi.org/10.1098/rspa.2012.0020.

[42] M. Schmuck, M. Pradas, G. A. Pavliotis, and S. Kalliadasis, *Derivation of effective macroscopic Stokes–Cahn–Hilliard equations for periodic immiscible flows in porous media*, Nonlinearity, 26 (2013), pp. 3259–3277, https://doi.org/10.1088/0951-7715/26/12/3259.

[43] R. Schulz, N. Ray, F. Frank, H. S. Mahato, and P. Knabner, *Strong solvability up to clogging of an effective diffusion-precipitation model in an evolving porous medium*, Eur. J. Appl. Math., 28 (2017), pp. 179–207, https://doi.org/10.1017/S0956792516000164.

[44] C. van Duijn and P. Knabner, *Travelling wave behaviour of crystal dissolution in porous media flow*, Eur. J. Appl. Math., 8 (1997), pp. 49–72.

[45] C. J. van Duijn, A. Mikelić, I. S. Pop, and C. Rosier, *Effective dispersion equations for reactive flows with dominant Péclet and Damkohler numbers*, in Advances in Chemical Engineering, G. B. Marin, D. West, and G. S. Yablonsky, eds., Adv. Chem. Eng. 34, Academic

Press, New York, 2008, pp. 1–45, https://doi.org/10.1016/S0065-2377(08)00001-X.
[46] C. J. van Duijn and I. S. Pop, *Crystal dissolution and precipitation in porous media: Pore scale analysis*, J. Reine Angew. Math., 577 (2004), pp. 171–211, https://doi.org/10.1515/crll.2004.2004.577.171.
[47] T. L. van Noorden, *Crystal precipitation and dissolution in a porous medium: Effective equations and numerical experiments*, Multiscale Model. Simul., 7 (2009), pp. 1220–1236, https://doi.org/10.1137/080722096.
[48] T. L. van Noorden, *Crystal precipitation and dissolution in a thin strip*, Eur. J. Appl. Math., 20 (2009), pp. 69–91, https://doi.org/10.1017/S0956792508007651.
[49] T. L. van Noorden and C. Eck, *Phase field approximation of a kinetic moving-boundary problem modelling dissolution and precipitation*, Interfaces Free Boundaries, 13 (2011), pp. 29–55, https://doi.org/10.4171/IFB/247.
[50] T. L. van Noorden and I. S. Pop, *A Stefan problem modelling crystal dissolution and precipitation*, IMA J. Appl. Math., 73 (2008), pp. 393–411, https://doi.org/10.1093/imamat/hxm060.
[51] T. L. van Noorden, I. S. Pop, and M. Röger, *Crystal dissolution and precipitation in porous media: L^1-contraction and uniqueness*, in Discrete Contin. Dyn. Syst., Dynamical Systems and Differential Equations, Proceedings of the 6th AIMS International Conference, suppl., 2007, pp. 1013–1020, https://doi.org/10.3934/proc.2007.2007.1013.
[52] S. Whitaker, *The Method of Volume Averaging*, Theory Appl. Transp. Porous Media 13, Springer Netherlands, 1999, https://doi.org/10.1007/978-94-017-3389-2.
[53] B. D. Wood, *Inertial effects in dispersion in porous media*, Water Resour. Res., 43 (2007), W12S16, https://doi.org/10.1029/2006WR005790.
[54] B. D. Wood, F. Golfier, and M. Quintard, *Dispersive transport in porous media with biofilms: Local mass equilibrium in simple unit cells*, Internat. J. Environ. Waste Manag., 7 (2011), pp. 24–48, https://doi.org/10.1504/IJEWM.2011.037364.
[55] Z. Xu and P. Meakin, *Phase-field modeling of solute precipitation and dissolution*, J. Chem. Phys., 129 (2008), 014705, https://doi.org/10.1063/1.2948949.